Fig. 3

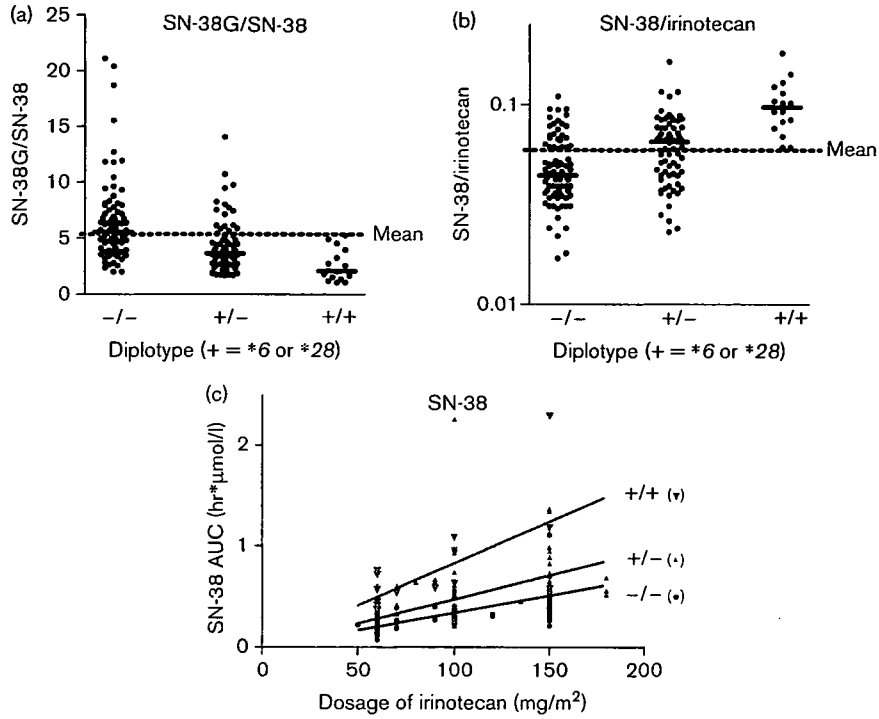

Effects of the genetic marker of *UGT1A1* '*6 or *28' on the area under concentration curve (AUC) ratios of SN-38G/SN-38 (a) and SN-38/irinotecan (b), and SN-38 by irinotecan dosage (c) in 176 Japanese cancer patients after irinotecan treatment.

Table 5 Association of *UGT1A1*6* and *28 with irinotecan toxicities

Diplotype (+ =*6 or *28)	Number of patients	Diarrhea (grade 3)	Neutropenia (grade 3 or 4)
Irinotecan monotherapy			
-/-	21	3 (14.3%)[a]	3 (14.3%)
+/-	29	2 (6.90%)	7 (24.1%)
+/+	5	1 (20.0%)	4 (80.0%)
P-value[b]		0.8500	**0.0117**
P-value[c]		0.3889	**0.0124**
With cisplatin			
-/-	35	1 (2.9%)	20 (57.1%)
+/-	20	2 (10.0%)	14 (70.0%)
+/+	7	1 (14.3%)	7 (100%)
P-value[b]		0.1747	**0.0315**
P-value[c]		0.3886	0.0863

[a]Percentage of the patient number in each diplotype is indicated in parentheses.
[b]Chi-squared test for trend.
[c]Fisher's exact test, (-/- and +/-) vs. +/+.

Table 6 Multiple regression analysis of the nadir of absolute neutrophil counts in the patients with irinotecan monotherapy

Variable	Coefficient	F-value	*P*-value	R^2	Intercept	*N*
				0.3942	643	53
Serum ALP[a]	-349.9	12.2	0.0010			
Neutrophil count before irinotecan treatment	0.2466	13.5	0.0006			
*6 or *28	-369.1	6.40	0.0146			

[a]Grade 1 or greater scores of serum ALP before irinotecan treatment.

of diarrhea in the irinotecan/capecitabine regimen, in which diarrhea was a major toxicity [20]. A highly frequent allele *1A9*22* with an insertion of T into the nine T repeats in the promoter region (-126_-118T_9 > T_{10}) was shown to have an enhanced promoter activity in an in-vitro reporter assay [21], whereas 1A9 protein expression levels did not change in the clinical samples [22]. Rare variations, *1A9*5* [766G > A(D256N)] and *UGT1A10*3* [605C > T(T202I)], were shown to cause reduced activity *in vitro*, but their clinical importance is still unknown [23,24]. Moreover, close linkages among *1A9*, *1A7*, and *1A1* polymorphisms were found in Caucasians and Asians in an ethnic-specific manner [20,25–28].

Our study also revealed close linkages between *1A9*22* and *1A7*1*, *1A7*3* and *1A1*6* or *28 [28]. This fact makes it difficult to draw firm conclusions about the effects of *1A7*3* and *1A9*22* themselves. It is, however, reasonable to conclude that the degree of neutropenia depends on the activity of UGT1A1, because UGT1A1 is a major UGT1A enzyme in the liver and plays a primary role for regulating plasma concentrations of SN-38.

Taken together, for practical application to individualized irinotecan therapy, genotyping of *UGT1A1*6* and *28 would be beneficial and necessary in Japanese cancer patients to avoid severe adverse reactions. The frequency

of homozygotes for '**6* or **28*' (namely, **6/*6*, **6/*28*, and **28/*28*) is approximately 10%, which is comparable to the frequency of **28* homozygotes in Caucasian populations. In our study, it may be difficult to establish definite guidelines for dose reductions of irinotecan for patients homozygous for '**6* or **28*'. Considering, however, 2.4-fold steep relationship between the dose of irinotecan and the AUC of SN-38 for patients homozygous for '**6* or **28*' compared with patients without '**6* or **28*' (Fig. 3c), the dose for patients homozygous for '**6* or **28*' should be reduced to a half of the dosage recommended for other patients. Prospective studies are necessary to confirm the validity of the recommendation for dose reduction in Japanese cancer patients homozygous for '**6 or *28*'.

Acknowledgements

We thank Ms Chie Sudo for her secretarial assistance. This study was supported in part by the Program for the Promotion of Fundamental Studies in Health Sciences and by the Program for the Promotion of Studies in Health Sciences of the Ministry of Health, Labor and Welfare of Japan. Analytical standards of irinotecan and its metabolites were kindly supplied by Yakult Honsha Co. Ltd. (Tokyo, Japan).

References

1 Garcia-Carbonero R, Supko JG. Current perspectives on the clinical experience, pharmacology, and continued development of the camptothecins. *Clin Cancer Res* 2002; **8**:641–661.
2 Slatter JG, Su P, Sams JP, Schaaf LJ, Wienkers LC. Bioactivation of the anticancer agent CPT-11 to SN-38 by human hepatic microsomal carboxylesterases and the in vitro assessment of potential drug interactions. *Drug Metab Dispos* 1997; **25**:1157–1164.
3 Iyer L, King CD, Whitington PF, Green MD, Roy SK, Tephly TR, *et al.* Genetic predisposition to the metabolism of irinotecan (CPT-11). Role of uridine diphosphate glucuronosyltransferase isoform 1A1 in the glucuronidation of its active metabolite (SN-38) in human liver microsomes. *J Clin Invest* 1998; **101**:847–854.
4 De Forni M, Bugat R, Chabot GG, Culine S, Extra JM, Gouyette A, *et al.* Phase I and pharmacokinetic study of the camptothecin derivative irinotecan, administered on a weekly schedule in cancer patients. *Cancer Res* 1994; **54**:4347–4354.
5 Gupta E, Lestingi TM, Mick R, Ramirez J, Vokes EE, Ratain MJ. Metabolic fate of irinotecan in humans: correlation of glucuronidation with diarrhea. *Cancer Res* 1994; **54**:3723–3725.
6 Hanioka N, Ozawa S, Jinno H, Ando M, Saito Y, Sawada J. Human liver UDP-glucuronosyltransferase isoforms involved in the glucuronidation of 7-ethyl-10-hydroxycamptothecin. *Xenobiotica* 2001; **31**:687–699.
7 Fisher MB, VandenBranden M, Findlay K, Burchell B, Thummel KE, Hall SD, *et al.* Tissue distribution and interindividual variation in human UDP-glucuronosyltransferase activity: relationship between UGT1A1 promoter genotype and variability in a liver bank. *Pharmacogenetics* 2000; **10**:727–739.
8 Ando Y, Saka H, Ando M, Sawa T, Muro K, Ueoka H, *et al.* Polymorphisms of UDP-glucuronosyltransferase gene and irinotecan toxicity: a pharmacogenetic analysis. *Cancer Res* 2000; **60**:6921–6926.
9 Iyer L, Das S, Janisch L, Wen M, Ramirez J, Karrison T, *et al.* UGT1A1*28 polymorphism as a determinant of irinotecan disposition and toxicity. *Pharmacogenomics J* 2002; **2**:43–47.
10 Innocenti F, Undevia SD, Iyer L, Chen PX, Das S, Kocherginsky M, *et al.* Genetic variants in the UDP-glucuronosyltransferase 1A1 gene predict the risk of severe neutropenia of irinotecan. *J Clin Oncol* 2004; **22**:1382–1388.
11 Marcuello E, Altes A, Menoyo A, del Rio E, Gomez-Pardo M, Baiget M. UGT1A1 gene variations and irinotecan treatment in patients with metastatic colorectal cancer. *Br J Cancer* 2004; **91**:678–682.
12 Rouits E, Boisdron-Celle M, Dumont A, Guerin O, Morel A, Gamelin E. Relevance of different UGT1A1 polymorphisms in irinotecan-induced toxicity: a molecular and clinical study of 75 patients. *Clin Cancer Res* 2004; **10**:5151–5159.
13 Kaniwa N, Kurose K, Jinno H, Tanaka-Kagawa T, Saito Y, Saeki M, *et al.* Racial variability in haplotype frequencies of UGT1A1 and glucuronidation activity of a novel single nucleotide polymorphism 686C>T (P229L) found in an African-American. *Drug Metab Dispos* 2005; **33**:458–465.
14 Sai K, Saeki M, Saito Y, Ozawa S, Katori N, Jinno H, *et al.* UGT1A1 haplotypes associated with reduced glucuronidation and increased serum bilirubin in irinotecan-administered Japanese patients with cancer. *Clin Pharmacol Ther* 2004; **75**:501–515.
15 Ciotti M, Basu N, Brangi M, Owens IS. Glucuronidation of 7-ethyl-10-hydroxycamptothecin (SN-38) by the human UDP-glucuronosyltransferases encoded at the UGT1 locus. *Biochem Biophys Res Commun* 1999; **260**:199–202.
16 Gagne JF, Montminy V, Belanger P, Journault K, Gaucher G, Guillemette C. Common human UGT1A polymorphisms and the altered metabolism of irinotecan active metabolite 7-ethyl-10-hydroxycamptothecin (SN-38). *Mol Pharmacol* 2002; **62**:608–617.
17 Oguri T, Takahashi T, Miyazaki M, Isobe T, Kohno N, Mackenzie PI. UGT1A10 is responsible for SN-38 glucuronidation and its expression in human lung cancers. *Anticancer Res* 2004; **24**:2893–2896.
18 Basu NK, Ciotti M, Hwang MS, Kole L, Mitra PS, Cho JW, *et al.* Differential and special properties of the major human UGT1-encoded gastrointestinal UDP-glucuronosyltransferases enhance potential to control chemical uptake. *J Biol Chem* 2004; **279**:1429–1441.
19 Ando M, Ando Y, Sekido Y, Ando M, Shimokata K, Hasegawa Y. Genetic polymorphisms of the UDP-glucuronosyltransferase 1A7 gene and irinotecan toxicity in Japanese cancer patients. *Jpn J Cancer Res* 2002; **93**:591–597.
20 Carlini LE, Meropol NJ, Bever J, Andria ML, Hill T, Gold P, *et al.* UGT1A7 and UGT1A9 polymorphisms predict response and toxicity in colorectal cancer patients treated with capecitabine/irinotecan. *Clin Cancer Res* 2005; **11**:1226–1236.
21 Yamanaka H, Nakajima M, Katoh M, Hara Y, Tachibana O, Yamashita J, *et al.* A novel polymorphism in the promoter region of human UGT1A9 gene (UGT1A9*22) and its effects on the transcriptional activity. *Pharmacogenetics* 2004; **14**:329–332.
22 Girard H, Court MH, Bernard O, Fortier LS, Villeneuve L, Hao Q, *et al.* Identification of common polymorphisms in the promoter of the UGT1A9 gene: evidence that UGT1A9 protein and activity levels are strongly genetically controlled in the liver. *Pharmacogenetics* 2004; **14**:501–515.
23 Jinno H, Saeki M, Saito Y, Tanaka-Kagawa T, Hanioka N, Sai K, *et al.* Functional characterization of human UDP-glucuronosyltransferase 1A9 variant, D256N, found in Japanese cancer patients. *J Pharmacol Exp Ther* 2003; **306**:688–693.
24 Jinno H, Saeki M, Tanaka-Kagawa T, Hanioka N, Saito Y, Ozawa S, *et al.* Functional characterization of wild-type and variant (T202I and M59I) human UDP-glucuronosyltransferase 1A10. *Drug Metab Dispos* 2003; **31**:528–532.
25 Kohle C, Mohrle B, Munzel PA, Schwab M, Wernet D, Badary OA, *et al.* Frequent co-occurrence of the TATA box mutation associated with Gilbert's syndrome (UGT1A1*28) with other polymorphisms of the UDP-glucuronosyltransferase-1 locus (UGT1A6*2 and UGT1A7*3) in Caucasians and Egyptians. *Biochem Pharmacol* 2003; **65**:1521–1527.
26 Huang MJ, Yang SS, Lin MS, Huang CS. Polymorphisms of uridine-diphosphoglucuronosyltransferase 1A7 gene in Taiwan Chinese. *World J Gastroenterol* 2005; **11**:797–802.
27 Innocenti F, Liu W, Chen P, Dedai AA, Das S, Ratain MJ. Haplotypes of variants in the UDP-glucuronosyltransferase 1A9 and 1A1 genes. *Pharmacogenet Genomics* 2005; **15**:295–301.
28 Saeki M, Saito Y, Jinno H, Sai K, Ozawa S, Kurose K, *et al.* Haplotype structures of the UGT1A gene complex in a Japanese population. *Pharmacogenomics J* 2006; **6**:63–75.
29 Sai K, Kaniwa N, Ozawa S, Sawada J. An analytical method for irinotecan (CPT-11) and its metabolites using a high-performance liquid chromatography: parallel detection with fluorescence and mass spectrometry. *Biomed Chromatogr* 2002; **16**:209–218.
30 Benjamini Y, Hochberg Y. Controlling the false discovery rate: a practical and powerful approach to multiple testing. *J Roy Stat Soc B* 1995; **57**:289–300.
31 Han JY, Lim HS, Shin ES, Yoo YK, Park YH, Lee JE, *et al.* Comprehensive analysis of UGT1A polymorphisms predictive for pharmacokinetics and treatment outcome in patients with non-small-cell lung cancer treated with irinotecan and cisplatin. *J Clin Oncol* 2006; **24**:2237–2244.
32 Kitagawa C, Ando M, Ando Y, Sekido Y, Wakai K, Imaizumi K, *et al.* Genetic polymorphism in the phenobarbital-responsive enhancer module of the UDP-glucuronosyltransferase 1A1 gene and irinotecan toxicity. *Pharmacogenet Genomics* 2005; **15**:35–41.

Population pharmacokinetic and pharmacodynamic analysis for time courses of docetaxel-induced neutropenia in Japanese cancer patients

Kazuhiro Ozawa,[1] Hironobu Minami[2] and Hitoshi Sato[1,3]

[1]Department of Clinical and Molecular Pharmacokinetics/Pharmacodynamics, School of Pharmaceutical Sciences, Showa University, 1-5-8 Hatanodai, Shinagawa-ku, Tokyo 142-8555; [2]The Division of Oncology/Hematology, National Cancer Center Hospital East, 6-5-1 Kashiwanoha, Kashiwa, Chiba 277-8577, Japan

(Received March 6, 2007/Revised July 26, 2007/Accepted August 8, 2007/Online publication September 20, 2007)

The present study describes a population pharmacokinetic and pharmacodynamic (PK/PD) analysis based on data obtained from cancer patients treated with docetaxel at the National Cancer Center Hospital East in Japan. Docetaxel was infused intravenously over 1 h every 3 weeks, and time courses of absolute neutrophil counts (ANC) for a total of 395 observations (62 patients) were analyzed using a semimechanistic-physiological PK/PD model in the NONMEM program. The prominent feature of our PK/PD model is that it has the capability to predict a temporary increase in ANC. Among 10 patient factors, α_1-acid glycoprotein was selected as a significant covariate for drug effect as the increase in α_1-acid glycoprotein was negatively correlated with the drug effect. Goodness-of-fit plots indicated that the model fitted well with the observed data, and the bootstrap method guaranteed robustness of the model. In conclusion, we developed a novel population PK/PD model that can adequately analyze ANC profiles after docetaxel administration in oncology practice, where temporary but consistent increases in ANC were observed. (*Cancer Sci* 2007; 98: 1985–1992)

Neutropenia occurs when most anticancer agents are used, and is often a dose-limiting factor. It is known that neutropenia correlates with the plasma or blood concentration of an anticancer drug. We have already reported the relationships between systemic drug exposure of docetaxel (i.e. area under the curve and the peak concentration at the end of infusion) and common toxicity criteria grade 4 neutropenia, using logistic regression analysis.[1]

Generally, anticancer drugs have a narrow therapeutic window, and interpatient variability in pharmacokinetics (PK) and pharmacodynamics (PD) may result in serious toxicities, including neutropenia.[2] A population PK/PD approach is a means to estimate the parameters of mean and interpatient variability of the PK/PD of drugs. A semimechanistic-physiological population PK/PD model of docetaxel was developed using data obtained from patients treated in clinical trials prior to drug registration.[3] This PK/PD model described myelosuppression following administration of cytotoxic agents. The model provides a simplified mathematical framework from the current conceptual knowledge of physiology to quantitatively mimic the underlying physiological process of hematopoiesis. The use of this PK/PD model allows a complete characterization of the entire absolute neutrophil count (ANC)–time profile from a sparse sampling scheme.

In clinical studies for the development of anticancer drugs, particular patients with moderate to severe liver dysfunction or poor performance status are commonly excluded, and PK/PD information from such patients is lacking. In the present study we developed a population PK/PD model using data from Japanese cancer patients treated with docetaxel, including patients with liver dysfunction or poor performance status, who should fall within exclusion criteria in clinical studies of drug development.

In our data, the ANC showed an increase in the early phase of docetaxel dosing. This increase may be caused by dexamethasone administered before the docetaxel regimen to prevent emesis. The increase in neutrophils caused by dexamethasone was previously reported *in vivo*.[4,5] Although the mechanisms underlying corticosteroid-induced neutrophil leukocytosis are not fully understood, leukocyte and endothelial cell adhesion molecule interactions are known to be a key to the movement of neutrophils within and out of the vasculature. Because the model of Friberg *et al.* has no capability to allow a temporary increase in ANC,[3] we modified that model to analyze our data. Briefly, an input compartment was added into the PD model to predict a temporary increase in ANC due to the effect of concomitant dexamethasone. As such, the current study extended the work of Friberg *et al.* by considering the effect of an increase in ANC as well as incorporating physiological covariates to explain between-patient variability.[3]

Materials and Methods

Patient selection. Sixty-two patients were enrolled into the present clinical research on docetaxel (as single-agent chemotherapy), executed in hospitals of the National Cancer Center Hospital East, Japan. Eligibility criteria included histologically or cytologically confirmed solid cancers against which docetaxel is active, age $\geq$ 20 years, Eastern Cooperative Oncology Group performance status 0–3, at least 3 weeks since last chemotherapy (6 weeks for mitomycin and nitrosoureas), and adequate hematological values (white blood cells $\geq$ 3000/μL, platelet count $\geq$ 75 000/μL). Exclusion criteria were active infection, severe heart disease, uncontrolled hypertension or diabetes mellitus, pregnant or nursing women, or seropositive for human immunodeficiency virus, hepatitis C virus, hepatitis B surface antigen, or syphilis. Patients who received granulocyte-colony stimulating factors after docetaxel administration were excluded from this analysis. This study was approved by the Institutional Review Board of the National Cancer Center Hospital East, Japan, and all patients gave written informed consent.

Treatment and follow-up. Docetaxel was infused intravenously over 1 h every 3 weeks. Most patients received the approved dose in Japan of 60 mg/m^2, but attending physicians were allowed to reduce the dose depending on liver function, performance status, or the extent of prior chemotherapy. Physical examination and toxicity assessment included blood chemistry and complete blood cell counts with differential counts as well as platelet counts, and were carried out before treatment and repeated

[3]To whom correspondence should be addressed. E-mail: sato-tky@umin.net

doi: 10.1111/j.1349-7006.2007.00615.x

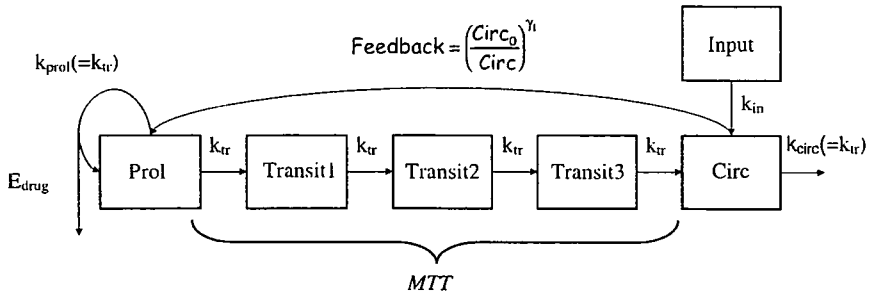

Fig. 1. The structure of the pharmacokinetic and pharmacodynamic model describing chemotherapy-induced myelosuppression for docetaxel.

at least weekly during the first course. Dexamethasone was administered before the docetaxel regimen to prevent emesis. Data on toxicity during the first course were used for PK/PD analysis in the present study.

Population PK analysis. Blood sampling for PK analysis was carried out before and 30 min during the docetaxel infusion, at the end of the infusion, and 0.17, 1, 5, 10, and 24 h after the end of infusion. Heparinized blood was centrifuged immediately, and plasma samples were frozen at −80°C until analysis. The concentration of docetaxel in plasma (total docetaxel) was determined by using a previously reported high-performance liquid chromatography method.[6] PK parameters for individuals were calculated by Bayesian estimation after population PK parameters were estimated in the entire population. These calculations were carried out using the NONMEM program (version V, level 1.1; GloboMax, Ellicot City, MD, USA). We used the method of First Order Conditional Estimation with the INTERACTION option. NONMEM was running with a Compaq Visual FORTRAN 6.6 compiler (Hewlett-Packard, Palo Alto, CA, USA) on a Pentium 4 central processing unit, under the Windows XP operating system (Microsoft Corporation, Redmond, WA, USA). A three-compartment open model with zero-order administration (i.e. constant intravenous infusion) and first-order elimination (ADVAN 11 and TRANS 4) was used to describe the plasma concentration–time course for docetaxel in the entire population. The PK model was parameterized in terms of clearance (CL), the volume of the central compartment (V_1), inter-compartment clearance between the central and peripheral-1 compartments (Q_2), the volume of the peripheral-1 compartment (V_2), inter-compartment clearance between the central and peripheral-2 compartments (Q_3), and the volume of the peripheral-2 compartment (V_3). Assuming a log-normal distribution for interindividual variability in PK parameters, the interindividual variability was modeled as (e.g. for clearance): $CL_j = CL \cdot \exp(\eta_{jCL})$, where CL_j and CL were the estimated values in an individual j and the population mean for clearance, respectively, and η_{jCL} was the individual random perturbation from the population mean. Intrapatient residual variability was also described by a proportional model.

Population PK and PD analyses. In the PD analysis, the time courses of ANC were analyzed for a total of 395 observations (62 patients). These calculations were carried out using the NONMEM program. We used the First Order method. We described a NONMEM control file using the ADVAN6 subroutine. Model selection was based on both a change in the minimum value of the objective function for nested models and a visual inspection of the goodness-of-fit plots. A nine-compartment semimechanistic-physiological PK/PD model consisting of three PK compartments and six PD compartments (Fig. 1) was used to characterize the time course of ANC following docetaxel administration. The present PD model, an extension of a model developed previously by Friberg *et al.*,[3] mimics physiological processes and consists of one compartment that represented stem cells and progenitor cells (i.e. proliferative cells 'Prol'), three transit compartments with maturing cells 'Transit1', 'Transit2', and 'Transit3', and a compartment of circulating observed blood cells, 'Circ', which represents the circulating neutrophils, and we added the compartment 'Input' to describe the increase in neutrophils in the early phase. A maturation chain of neutrophils, with transit compartments and rate constant (k_{tr}), allowed prediction of a time delay between administration and the observed effect. k_{tr} was related to the mean transit time (MTT) between the transit compartments as $MTT = (n+1)/k_{tr}$, where n was the number of maturation compartments. The generation of new cells in Prol was dependent on the number of cells in the compartment; that is, self renewal or mitosis, a proliferation rate constant determining the rate of cell division (k_{prol}), and a feedback mechanism from the circulating cells $(Circ_0/Circ)^{\gamma_1}$, where $Circ_0$ was the baseline value of Circ and γ_1 represented a feedback parameter. The input rate constant (k_{in}) determined the rate of input from the input compartment to the circulation compartment, and was related to the mean input time (MIT) as $MIT = 1/k_{in}$. The differential equations governing the semimechanistic-physiological PD model were as follows:

$$dProl/dt = k_{prol} \cdot Prol \cdot (1 - E_{drug}) \cdot (Circ_0/Circ)^{\gamma_1} - k_{tr} \cdot Prol \quad (1)$$

$$dTransit1/dt = k_{tr} \cdot Prol - k_{tr} \cdot Transit1 \quad (2)$$

$$dTransit2/dt = k_{tr} \cdot Transit1 - k_{tr} \cdot Transit2 \quad (3)$$

$$dTransit3/dt = k_{tr} \cdot Transit2 - k_{tr} \cdot Transit3 \quad (4)$$

$$dInput/dt = -k_{in} \cdot Input \quad (5)$$

$$dCirc/dt = k_{tr} \cdot Transit3 + k_{in} \cdot Input - k_{circ} \cdot Circ \quad (6)$$

where E_{drug} was defined as a linear function of the drug concentration in the central compartment (CP) using a drug-effect parameter, $SLOPE$, as follows:

$$E_{drug} = SLOPE \cdot CP \quad (7)$$

For numerically solving the above equations, each compartment's initial value was set as follows: Prol ($t = 0$) = Transit1 ($t = 0$) = Transit2 ($t = 0$) = Transit3 ($t = 0$) = Circ ($t = 0$), where Circ ($t = 0$) was fixed at its observed value, and Input ($t = 0$) = $IP0$, where $IP0$ was estimated as a parameter. At steady state, dProl/dt = 0, and therefore $k_{prol} = k_{tr}$. To minimize the number of parameters to be estimated, it was assumed in the modeling that $k_{circ} = k_{tr}$. Gamma1 (γ_1) quantified the strength of the feedback action from the colony-stimulating factors that regulated the physiological process. Interindividual variability models were examined assuming log-normal distribution of individual MTT, $SLOPE$, and $IP0$. These equations are presented as follows:

$$MTT_j = \theta_{MTT} \cdot \exp(\eta_{jMTT}) \quad (8)$$

$$Slope_j = \theta_{Slope} \cdot \exp(\eta_{jSlope}) \quad (9)$$

$$IP0_j = \theta_{IP0} \cdot \exp(\eta_{jIP0}) \quad (10)$$

The intraindividual variability was modeled with an additive and proportional component in the report by Friberg *et al.*,[3] but this model did not converge with our data. Therefore, we applied an exponential model (i.e. a log-normal distribution model) as the

doi: 10.1111/j.1349-7006.2007.00615.x

intraindividual variability term. The estimated PD parameters were *MTT*, *Slope*, γ_1, *MIT*, and *IP0*, and interindividual variability (η) was assumed for *MTT*, *Slope*, and *IP0*.

Relationships between covariates and PD parameters. Patient-specific factors that could affect PD parameters (*MTT*, *SLOPE*, and *IP0*) were evaluated as potential covariates using both linear and non-linear models.

Patient factors considered as potential covariates with respect to each of the PD model parameters included the following continuous variables: age, albumin, body surface area, creatinine clearance, total bilirubin, α_1-acid glycoprotein (AGP), and platelets. Categorical variables included sex, performance status, and previous cytotoxic chemotherapy (=3 regimens or not). Because overall neutropenic response is a function of all model parameters, each potential covariate was tested for relationships with *MTT*, *SLOPE*, and *IP0*. Continuous variables were normalized by their population median and were expressed by both linear additive and multiplicative models. Linear additive models were coded as $P = \beta_1 + \beta_2 \cdot \mathrm{COV}$, and multiplicative models were coded as $P = \beta_1 \cdot \mathrm{COV}^{\beta_2}$, where P was the individual's estimate of the parameters, β_1 represented the typical value of the parameter, β_2 represented the effect of the covariate, and COV was the ratio of the individual's covariate value to the median value. To identify potentially significant factors affecting the PD parameters, we used graphical diagnostics and the objective function values (OVF) in the likelihood ratio test. Differences in objective function values obtained by comparing each model were distributed asymptotically as χ^2 with degrees of freedom equal to the difference in the number of parameters between the two models. Potentially significant covariates were identified as those factors that, when added to the base model individually, resulted in a decrease in the objective function of 3.84 points or more ($P \leq 0.05$ based on a χ^2 distribution with 1 degree of freedom). Potential covariates were added to the model sequentially, based on the change in objective function for the individual covariate; those covariates that reduced the objective function by the greatest amount were added to the model first. Potential covariates that did not result in a decrease in the objective function of 3.84 points or more on sequential addition to the model were removed from the analysis. When a full model had been established, the process was then reversed, with each potential covariate being removed individually from the full model. Covariates retained in the final model were those associated with a significant increase (≤10.8 points for 1 degree of freedom, $P < 0.001$) in the minimum value of OVF when removed from the full model.

Bootstrap validation. The accuracy and robustness of the final model were assessed by using a bootstrap method.[7] The bootstrap method was first presented by Efron,[8] and a very informative account is provided by Efron and Tibshirani.[9] A bootstrap sample was generated by repeated random sampling from the original data set, and the size of bootstrap sample was the same as the original sample size. Two hundred bootstrap samples were reconstructed, and the final model was fitted repeatedly to the 200 bootstrap samples. The mean parameter estimates obtained from bootstrap replications, which were calculated normally, were compared with those obtained from the original data set.

Results

The characteristics of the 62 patients treated in the present study are listed in Table 1. Forty-four patients had breast cancer. Ten patients had non-small cell lung cancer. Three patients had head and neck cancer. Five patients had other types of cancer. Fig. 2 shows ANC used for the population PD analysis. The basic structural PK/PD model included interindividual variabilities for *MTT*, *SLOPE*, and *IP0*, and an exponential residual error term. AGP was selected as a significant covariate ($P < 0.001$) for *SLOPE*, and the multiplicative model in which the decrease in *SLOPE* was in accordance with the increase in AGP was the most significant. Table 2 shows the parameter estimates of the population PK model including the population mean (θ) and magnitude of interindividual variability (ω), and the magnitude of

Table 1. Characteristics of the 62 patients in the present study

Patients' characteristics	Median and range or no.
Age (years)	55.5 (21–77)
Sex (female/male)	51/11
Performance status (PS) (0/1/2/3)	14/36/7/5
Regimens of prior chemotherapy (*n*)	
<3	46
≥3	16
Disease (BC/NSCLC/H-N/others)	44/10/3/5
Albumin (g/dL)	3.7 (2.6–4.5)
Total bilirubin (mg/dL)	0.6 (0.2–1.2)
Aspartate aminotransferase (IU/L)	24 (11–310)
Alanine aminotransferase (IU/L)	20 (6–140)
Alkaline phosphatase (IU/L)	249 (93–1382)
Creatinine (mg/dL)	0.6 (0.4–1.3)
α1-Acid glycoprotein (mg/dL)	90 (51–241)
Dose (mg/m²)	
PS0	60 (39–60)
PS1	60 (40–63)
PS2	60 (58–62)
PS3	30 (26–60)

BC, breast cancer; H-N, head and neck cancer; NSCLC, non-small cell lung cancer.

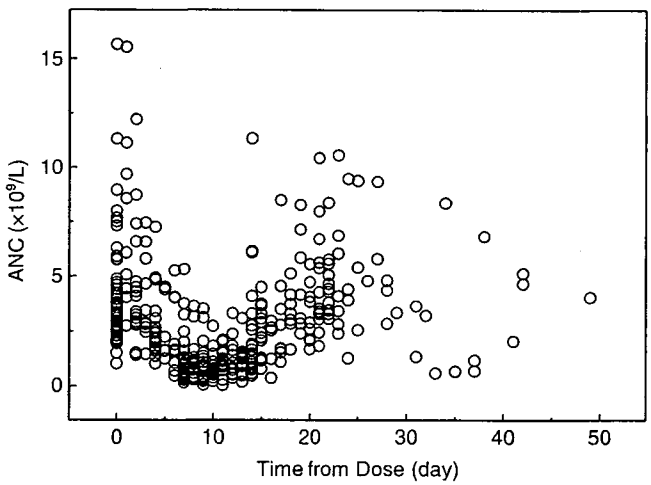

Fig. 2. Time after administration versus observed absolute neutrophil count.

Table 2. Estimated parameters of the population pharmacokinetic model

Parameter	Estimate	Standard error
θ_{CL} (L/h)	35.7	1.30
θ_{V1} (L)	6.94	0.303
θ_{Q2} (L/h)	5.58	0.356
θ_{V2} (L)	7.39	1.08
θ_{Q3} (L/h)	12.5	1.22
θ_{V3} (L)	225	46.2
ω_{CL}	39.9†	0.027
ω_{V1}	26.4†	0.025
σ	26.8†	0.085

†Expressed as coefficient of variance (CV)%.

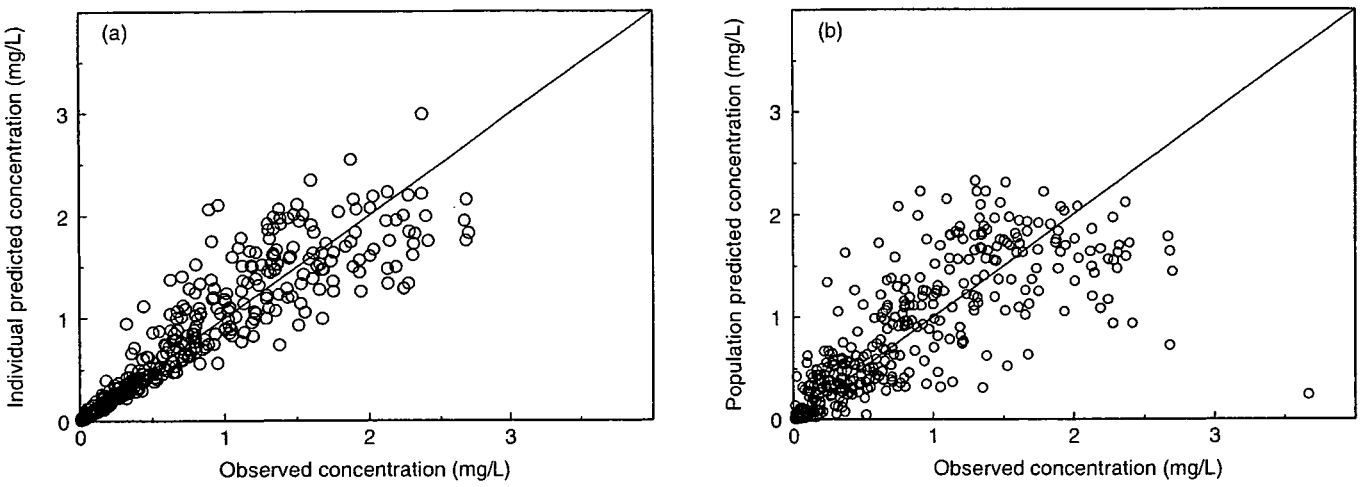

Fig. 3. (a) Observed docetaxel concentration versus predicted docetaxel concentration from a Bayesian post hoc analysis of the model. The solid line represents the unit line. (b) Observed docetaxel concentration versus predicted docetaxel concentration from population mean parameters of the model. The solid line represents the unit line.

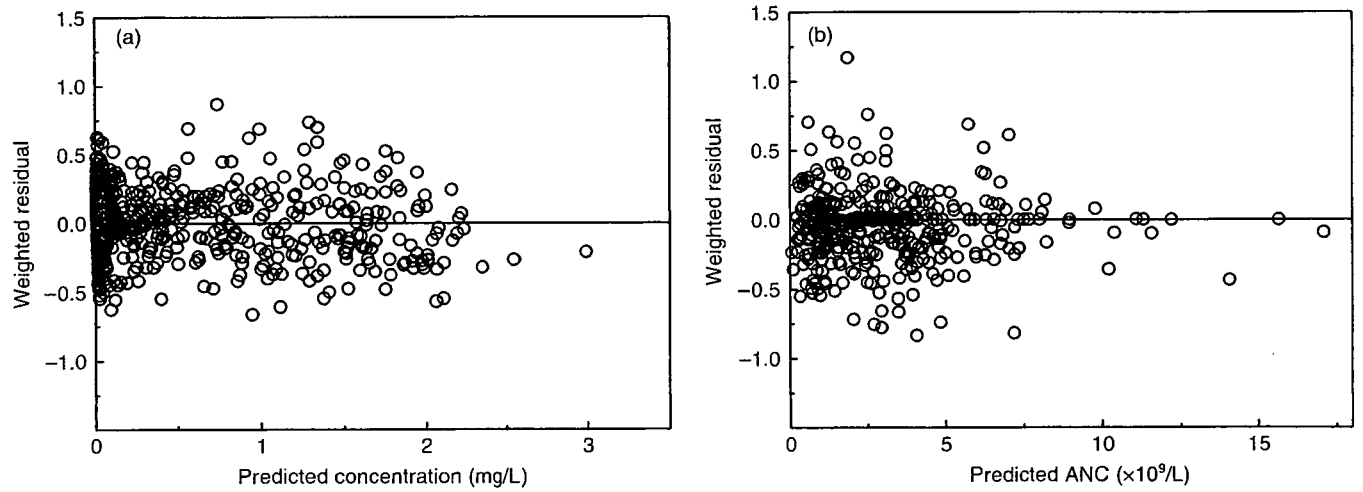

Fig. 4. (a) Weighted residuals versus predicted concentration. The horizontal line represents the zero level. (b) Weighted residuals versus predicted absolute neutrophil count. The horizontal line represents the zero level.

Table 3. Estimated parameters of the final model

Parameter	Estimate	Standard error
θ_{MTT} (h)	113	4.62
θ_{SLOPE}	17.9	1.75
$\theta_{\gamma 1}$	0.196	0.013
θ_{MIT} (h)	35.5	5.08
θ_{IP0} (×10⁹)	5.19	1.51
$\theta_{\gamma 2}$	−1.38	0.287
ω_{MTT}	11.1†	0.005
ω_{SLOPE}	68.2†	0.143
ω_{IP0}	110†	0.629
σ	29.1†	0.013

†Expressed as coefficient of variance (CV)%.

intraindividual variability (σ). Figs 3a,b and 4a show the goodness-of-fit plots for the population PK analysis. The value of θ_{CL} was determined to be 35.7 and similar to that in a previous study (38.5) reported by Bruno *et al.*[10] Table 3 shows the parameter estimates of the final regression model. In the final regression model, *SLOPE* was modeled with a covariate as follows, whereas the other equations (1–6) remained the same:

$$SLOPE = \theta_{Slope} \cdot \left(\frac{AGP}{AGP_{median}} \right)^{\gamma_2} \quad (11)$$

The addition of AGP onto *SLOPE* decreased the interindividual variability in *SLOPE* from 86.3 to 69.6%. In order to confirm whether or not the final model actually reflected the observed ANC, we created three plots (Figs 4b,5a,b). Weighted residual plots for the final model are shown in Fig. 4b. The predicted values obtained by Bayesian estimation were plotted versus the observed values in Fig. 5a, and the predicted values obtained by population mean parameters were plotted versus the observed values in Fig. 5b. The values were generally distributed around zero and were relatively symmetric. No obvious bias pattern was apparent in the plot of the predicted concentration versus the weighted residual. Table 4 lists the parameter estimates of the final model and the results of the bootstrap validation step. As a result of analyzing 200 bootstrap samples, 166 samples were converged. All structural parameters (θ_i) and the variance

doi: 10.1111/j.1349-7006.2007.00615.x

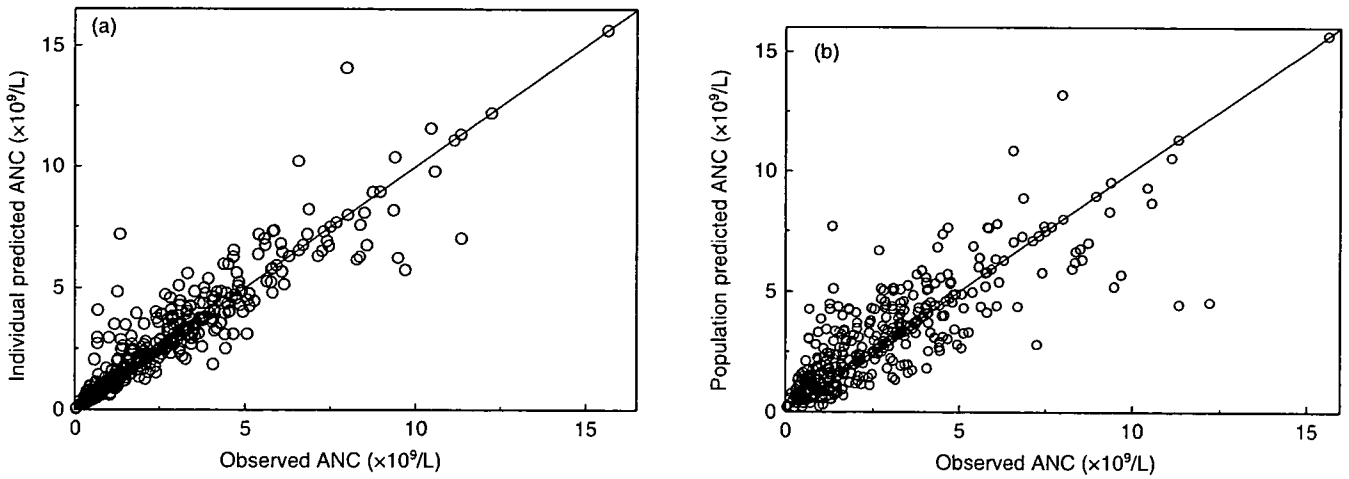

Fig. 5. (a) Observed absolute neutrophil count (ANC) versus predicted ANC from a Bayesian post hoc analysis of the final model. The solid line represents the unit line. (b) Observed ANC versus predicted ANC from population mean parameters of the final model. The solid line represents the unit line.

Table 4. Bootstrap validation of the final model

Parameter	Final model (SE)†	Bootstrap mean(SE)‡	Difference (%)§
θ_{MTT}	113 (4.62)	112 (0.837)	1.12
θ_{SLOPE}	17.9 (1.75)	19.3 (0.258)	−7.90
$\theta_{\gamma 1}$	0.196 (0.013)	0.196 (0.002)	0.049
θ_{MIT}	35.9 (5.08)	39.0 (2.34)	−9.93
θ_{IP0}	5.19 (1.51)	5.68 (0.156)	−9.38
$\theta_{\gamma 2}$	−1.38 (0.287)	−1.08 (0.034)	21.6
ω_{MTT}	11.1¶ (0.005)	11.2¶ (0.003)	−0.766
ω_{SLOPE}	68.2¶ (0.143)	65.8¶ (0.010)	3.46
ω_{IP0}	110¶ (0.629)	100¶ (0.035)	8.80
σ	29.1¶ (0.013)	28.5¶ (0.002)	2.19

†Obtained from the original data set. ‡Calculated from 200 bootstrap replicates (166 convergence). §(final model value-bootstrap value)/final model value × 100%. ¶Expressed as coefficient of variance (CV)%.

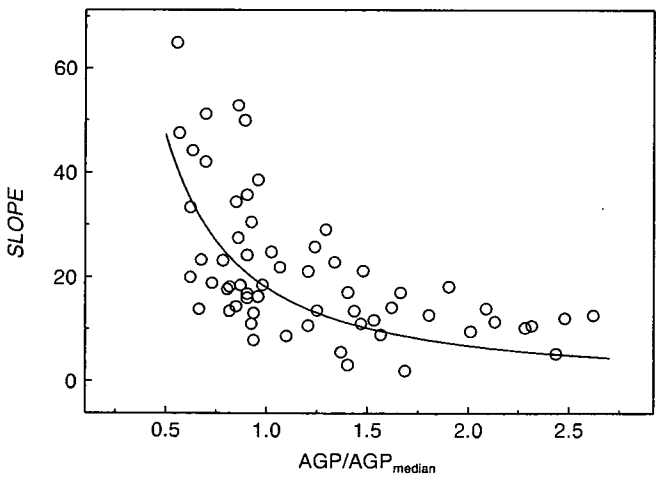

Fig. 6. Relationship between α_1-acid glycoprotein (AGP) and slope. Circles show slope estimated by Bayesian estimation. The line shows the theoretical value from the final model.

parameters (ω, σ) were within 21.6% of the bootstrapped mean out of the 166 samples. Fig. 6 shows the relationship between AGP and *SLOPE* calculated by Bayesian estimation for each individual patient.

Discussion

In the present study, a semimechanistic-physiological population PK/PD model was applied for the first time to analyze the data from Japanese cancer patients treated with docetaxel. The goodness-of-fit plots (Figs 3a,b,4a) for the population PK analysis indicated that a three-compartment open model was fitted well with the observed data. For the population PD analysis of the ANC data, we preliminarily carried out an analysis using the same model as that reported by Friberg *et al.*[3] to evaluate differences in drug-effect parameters in comparison with the previous study. The magnitude of the population mean of drug-effect, θ_{SLOPE}, was determined to be 15.3, and larger than that (8.58) obtained in the previous study, implying that the patients who entered into this study were more sensitive to docetaxel-induced neutropenia due to our inclusion criteria that allowed severe liver dysfunction and poor performance status.

Subsequently, we came to modify the model of Friberg *et al.*[3] to better simulate the ANC time courses, because we observed a temporary but obvious increase in ANC at the initial phase after docetaxel dosage in approximately 30% of the subjects. Such an increase in neutrophil counts that was considered to be caused by premedication of dexamethasone was previously reported *in vivo*.[4,5] Although the mechanisms underlying corticosteroid-induced neutrophil leukocytosis are not fully understood, leukocyte and endothelial cell adhesion molecule interactions are known to be key to the movement of neutrophils within and out of the

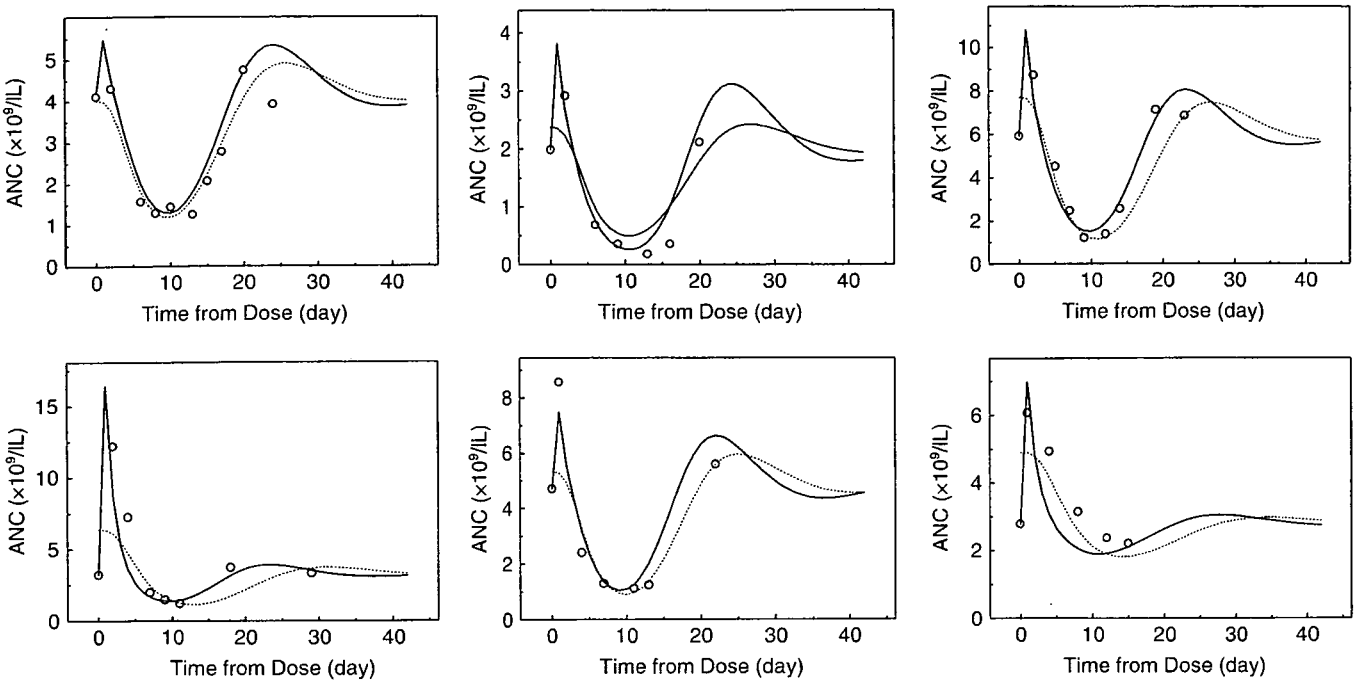

Fig. 7. Absolute neutrophil count (ANC) versus time for representative treatment cycles based on the final docetaxel-ANC pharmacokinetic and pharmacodynamic model. Open circles represent the ANC data taken from Japanese cancer patients used in the present study. Solid curves are fitted by our model. The dotted curves are fitted by the model of Friberg *et al.*[3]

vasculature. Crockard *et al.* reported an association between an increase in neutrophil counts and a reduction in neutrophil adhesion molecules (L-selectin and Mac-1) after methylprednisolone dosage.[11] From these lines of evidence, we added a model capability to allow such a temporary increase in ANC into the model of Friberg *et al.*[3]

Absolute neutrophil count decreased with the administration of docetaxel, reached a nadir at approximately 1 week after the dosage, and increased thereafter. We then observed that ANC increased to a level higher than the basal ANC value 3–4 weeks after docetaxel dosage, consistent with the report of Friberg *et al.*[3] Therefore, our model incorporated a feedback mechanism to describe this rebound (or overshoot) phenomenon, as was done in their study. It was assumed that the proliferative rate was negatively correlated with Circ, and the effect of feedback ceased when Circ returned to the basal ANC value ($Circ_0$) in such a way that the proliferative rate contained the feedback factor of $(Circ/Circ_0)^{\gamma}$.

Friberg *et al.* previously reported a semimechanistic-physiological population PK/PD model, where drug effect was presented by a linear model, $SLOPE \cdot CP$.[3] We preliminarily tested an Emax model where drug effect was represented as $Emax \cdot CP/(EC50 \cdot CP)$ (Emax is the maximum drug effect and EC50 is the plasma concentration when the drug effect falls in the half of Emax.) However, this model did not significantly reduce the OVF compared with the linear model. Therefore, we adopted $SLOPE \cdot CP$ as the model of drug effect.

Our model can be viewed as an extension of the model of Friberg *et al.*[3] To compare the present and previous models, we used OVF in the likelihood ratio test. In spite of adding one parameter, our model decreased OVF of 250.880 points ($P < 0.001$ based on a χ^2 distribution with 1 degree of freedom). This indicates that our model can be fitted better than the model of Friberg *et al.*[3] Fig. 7 shows the typical profiles of the ANC, which show a comparison between our model and that of Friberg *et al.*[3] There was a tendency for the prediction error to be larger when Friberg *et al.*'s model was fitted for the data of ANC, which exhibited an increase at the initial phase. Because the previous model had no capability to allow a temporary increase in ANC, the model fitting was adjusted by overpredicting the initial ANC value at time zero, and underpredicting the peak ANC value. However, it is important to predict the time profile that characterizes depth and duration of decrease in ANC (i.e. the nadir of the ANC [NANC] and the time of its occurrence after drug administration [T_{Nadir}]). As inspected typically from Fig. 7, the predictability of our model for NANC and T_{Nadir} was sufficiently good, but there seemed to be little difference between previous models and our model in terms of the predictability for NANC and T_{Nadir}. It is thus suggested that our model is comparable to that of Friberg *et al.*[3] with respect to the prediction of the presence or absence of neutropenia as well as the timing of its occurrence.

In our study, we evaluated potential covariates for PD parameters (i.e. *MTT*, *SLOPE*, and *IP0*), and AGP was selected as a significant covariate for *SLOPE* with the multiplicative model in which *SLOPE* decreased according to the increase in AGP. Population PK/PD analysis of docetaxel using total drug concentrations previously reported that high serum levels of AGP were significantly associated with low clearance of total docetaxel as well as mild neutropenia and diminished antitumor efficacy.[10,12,13] AGP is a major binding protein of docetaxel, and it is estimated that 29% of the docetaxel in plasma is bound to AGP, whereas the fraction bound by albumin is 20%.[14] This may be considered to account for the correlation between serum levels of AGP and clearance of the drug.[10,13] However, patients with acute-phase reactions were suggested to have reduced activity of CYP3A4,[15,16] which may also explain the association between high serum levels of AGP and low clearance of docetaxel. With regard to the mechanism of the association between AGP levels and the toxicity or antitumor activity in the population PD analysis,[10,12,13,15–17] high AGP levels might be associated with low concentrations of unbound docetaxel and therefore with milder toxicity but decreased antitumor activity. However, a previous population PK/PD study of docetaxel using unbound drug concentrations reported that the level of AGP determined not only the PK but

doi: 10.1111/j.1349-7006.2007.00615.x

also the PD of docetaxel.[1] Although the mechanisms underlying the influence of AGP for the PD of docetaxel are not fully understood, it may be considered as one of the reasons that AGP is an acute-phase protein and its expression is induced by cytokines such as tumor necrosis factor, which also induces various other cytokines including granulocyte-stimulating factors.[18–20] These lines of evidence suggest that AGP was selected as a covariate of *SLOPE* (i.e. drug effect) due to its influence on both the PK and PD aspects of docetaxel.

Goodness-of-fit plots (Figs 4b,5) indicated that the final model was fitted well with the observed data, and Table 4 indicates that the convergence ratio on bootstrap data was so high that the robustness of this model was sufficiently guaranteed. The differences between θ_i of the final-model estimates and θ_i of the bootstrap means were relatively small, except for $\theta_{\gamma 2}$ (difference 21.6%). In order to evaluate the effects of this $\theta_{\gamma 2}$ difference on *SLOPE*, *SLOPE* was estimated using the final model when $\theta_{\gamma 2}$ was set at a fixed value of the bootstrap mean. As a result, *SLOPE* was hardly affected by setting $\theta_{\gamma 2}$ to a fixed bootstrap mean. Therefore, the parameter estimates on bootstrap samples corresponded well with the original data.

In conclusion, we developed a modified semimechanistic-physiological population PK/PD model that can adequately analyze the ANC profiles after docetaxel administration to patients in real clinical settings, where temporary but consistent increases in the ANC were observed. This model may be useful in clinical settings where the Bayesian estimation approach may be carried out using one or two initial ANC data in the early phase of cancer chemotherapy.

Acknowledgments

We greatly appreciate helpful discussion with Mr Akiyuki Suzuki, the division of Clinical Pharmacology, Pfizer Japan.

References

1 Minami H, Kawada K, Sasaki Y *et al.* Pharmacokinetics and pharmacodynamics of protein-unbound docetaxel in cancer patients. *Cancer Sci* 2006; **97**: 235–41.
2 Ratain MJ, Schilsky RL, Conley BA, Egorin MJ. Pharmacodynamics in cancer therapy. *J Clin Oncol* 1990; **8**: 1739–53.
3 Friberg LE, Henningsson A, Maas H, Nguyen L, Karlsson MO. Model of chemotherapy-induced myelosuppression with parameter consistency across drugs. *J Clin Oncol* 2002; **20**: 4713–21.
4 Denison FC, Elliott CL, Wallace EM. Dexamethasone-induced leucocytosis in pregnancy. *Br J Obstet Gynaecol* 1997; **104**: 851–3.
5 Mishler JM, Emerson PM. Development of neutrophilia by serially increasing doses of dexamethasone. *Br J Haematol* 1977; **36**: 249–57.
6 Vergniol J, Bruno R, Montay G, Frydman A. Determination of Taxotere in human plasma by a semi-automated high-performance liquid chromatographic method. *J Chromatogr* 1992; **582**: 273–8.
7 Ette EI. Stability and performance of a population pharmacokinetic model. *J Clin Pharmacol* 1997; **37**: 486–95.
8 Efron B. Bootstrap methods: another look at the jackknife. *Ann Stat* 1979; **7**: 1–26.
9 Efron B, Tibshirani R. Bootstrap methods for standard errors, confidence intervals, and other measures of statistical accuracy. *Stat Sci* 1986; **1**: 54–77.
10 Bruno R, Vivier N, Vergniol JC, Phillips SLD, Montay G, Sheiner LB. A population pharmacokinetic model for docetaxel (Taxotere), model building and validation. *J Pharmacokin Biopharm* 1996; **24**: 153–72.
11 Crockard AD, Boylan MT, Droogan AG, McMillan SA, Hawkins SA. Methylprednisolone-induced neutrophil leukocytosis – down-modulation of neutrophil l-selectin and Mac-1 expression and induction of granulocyte-colony stimulating factor. *Int J Clin Laboratory Res* 1998; **28**: 110–15.
12 Bruno R, Hille D, Riva A. Population pharmacokinetics/pharmacodynamics of docetaxel in phase II studies in patients with cancer. *J Clin Oncol* 1998; **16**: 187–96.
13 Loos WJ, Baker SD, Verweij J, Boonstra JG, Sparreboom A. Clinical pharmacokinetics of unbound docetaxel, role of polysorbate 80 and serum proteins. *Clin Pharmacol Ther* 2003; **74**: 364–71.
14 Urien S, Barre J, Morin C, Paccaly A, Montay G, Tillement J-P. Docetaxel serum protein binding with high affinity to α1-acid glycoprotein. *Invest New Drugs* 1996; **14**: 147–51.
15 Rivory L, Slaviero K, Clarke S. Hepatic cytochrome P450 3A drug metabolism is reduced in cancer patients who have an acute-phase response. *Br J Cancer* 2002; **87**: 277–80.
16 Baker SD, Schaik RH, Nv Rivory LP. Factors affecting cytochrome P-450 3A activity in cancer patients. *Clin Cancer Res* 2004; **10**: 8341–50.
17 Bruno R, Olivares R, Berille J. α-1-Acid glycoprotein as an independent predictor for treatment effects and a prognostic factor of survival in patients with non-small cell lung cancer treated with docetaxel. *Clin Cancer Res* 2003; **9**: 1077–82.
18 Baumann H, Gauldie J. The acute response. *Immunol Today* 1994; **15**: 74–80.
19 Koeffler P, Gasson J, Ranyard J, Souza L, Shepard M, Munker R. Recombinant human TNFα stimulates production of granulocyte colony stimulating factor. *Blood* 1987; **70**: 55–9.
20 Seelentag WK, Mermod JJ, Montesano R, Vassalli P. Additive effects of interleukin 1 and tumour necrosis factor-α on the accumulation of the three granulocyte and macrophage colony-stimulating factor mRNAs in human endothelial cells. *EMBO J* 1987; **6**: 2261–5.

Appendix I

```
$PROBLEM ANC_PKPD_MODEL
$INPUT ID AMT CMT RATE TIME ANC = DV CL V1 Q2 V2 Q3 V3 BASE AGP1
$DATA DATA.csv
$SUBROUTINES ADVAN6 TOL = 3

$MODEL
COMP = (CENTRAL,DEFDOSE)
COMP = (PERIPH1)
COMP = (PERIPH2)
COMP = (INPUT2)
COMP = (POOL)
COMP = (DELAY1)
COMP = (DELAY2)
COMP = (DELAY3)
COMP = (OBS,DEFOBS)

$PK
K10 = CL/V1
K12 = Q2/V1
K21 = Q2/V2
K13 = Q3/V1
K31 = Q3/V3
```

```
MTT = THETA(1)*EXP(ETA(1))
KTR = 4/MTT
AGPm = 94
gam2 = THETA(6)
FSLOPE = (AGP/AGPm)** gam2
SLOPE = THETA(2)*FSLOPE*EXP(ETA(2))
gam = THETA(3)*EXP(ETA(3))
IPT = THETA(4)*EXP(ETA(4))
KIN = 1/IPT
IP0 = THETA(5)*EXP(ETA(5))
F4 = IP0

$DES
DADT(1) = -K10*A(1)-K12*A(1) + K21*A(2)-K13*A(1) + K31*A(3)
DADT(2) = -K21*A(2) + K12*A(1)
DADT(3) = -K31*A(3) + K13*A(1)
CP = A(1)/V1
EDRUG = SLOPE*CP

DADT(4) = -KIN*A(4)
DADT(5) = KTR*A(5)*(1-EDRUG)*(BASE/A(9))**gam-KTR*A(5)
DADT(6) = KTR*A(5)-KTR*A(6)
DADT(7) = KTR*A(6)-KTR*A(7)
DADT(8) = KTR*A(7)-KTR*A(8)
DADT(9) = KTR*A(8) + KIN*A(4)-KTR*A(9)

$ERROR
IPRD = F
IRES = ANC - F
W = F
IF(IPRD.EQ.0)W = 1
IWRES = IRES/W
Y = F*EXP(ERR(1))

$THETA (0,115,500) (0,13,100) (0,0.1,1) (0,30,200) (0,5,50)
       (,0.1)
$OMEGA 0.1
       0.1
       (0 FIXED)
       (0 FIXED)
       0.1
$SIGMA 0.1

$ESTIMATION SIG = 4 MAXEVAL = 9999 PRINT = 5 METHOD = 0 POSTHOC NOABORT
$COVR
```


doi: 10.1111/j.1349-7006.2007.00615.x

Drug Metab. Pharmacokinet. 22 (6): *SNP50* (456)-*SNP55* (461) (2007).

SNP Communication

*Genetic Variations and Frequencies of Major Haplotypes in SLCO1B1 Encoding the Transporter OATP1B1 in Japanese Subjects: SLCO1B1*17 is More Prevalent Than *15*

Su-Ryang KIM[1], Yoshiro SAITO[1,2,*], Kimie SAI[1,3], Kouichi KUROSE[1,4], Keiko MAEKAWA[1,2], Nahoko KANIWA[1,4], Shogo OZAWA[1,5,†], Naoyuki KAMATANI[6], Kuniaki SHIRAO[7], Noboru YAMAMOTO[7], Tetsuya HAMAGUCHI[7], Hideo KUNITOH[7], Yuichiro OHE[7], Yasuhide YAMADA[7], Tomohide TAMURA[7], Teruhiko YOSHIDA[8], Hironobu MINAMI[9,‡], Atsushi OHTSU[10], Nagahiro SAIJO[11] and Jun-ichi SAWADA[1,2]

[1]*Project Team for Pharmacogenetics,* [2]*Division of Biochemistry and Immunochemistry,*
[3]*Division of Biosignaling,* [4]*Division of Medicinal Safety Science,*
[5]*Division of Pharmacology, National Institute of Health Sciences, Tokyo, Japan*
[6]*Division of Genomic Medicine, Department of Advanced Biomedical Engineering and Science, Tokyo Women's Medical University, Tokyo, Japan*
[7]*Division of Internal Medicine, National Cancer Center Hospital,*
[8]*Genomics Division, National Cancer Center Research Institute, National Cancer Center, Tokyo, Japan*
[9]*Division of Oncology/Hematology,* [10]*Division of GI Oncology/Digestive Endoscopy,*
[11]*Deputy Director, National Cancer Center Hospital East, National Cancer Center, Chiba, Japan*

Full text of this paper is available at http://www.jstage.jst.go.jp/browse/dmpk

Summary: A liver-specific transporter organic anion transporting polypeptide 1B1 (OATP1B1, also known as OATP-C) is encoded by *SLCO1B1* and mediates uptake of various endogenous and exogenous compounds from blood into hepatocytes. In this study, 15 *SLCO1B1* exons (including non-coding exon 1) and their flanking introns were comprehensively screened for genetic variations in 177 Japanese subjects. Sixty-two genetic variations, including 28 novel ones, were found: 7 in the 5′-flanking region, 1 in the 5′-untranslated region (UTR), 13 in the coding exons (9 nonsynonymous and 4 synonymous variations), 5 in the 3′-UTR, and 36 in the introns. Five novel nonsynonymous variations, 311T>A (Met104Lys), 509T>C (Met170Thr), 601A>G (Lys201Glu), 1553C>T (Ser518Leu), and 1738C>T (Arg580Stop), were found as heterozygotes. The allele frequencies were 0.008 for 1738C>T (Arg580Stop) and 0.003 for the four other variations. Arg580Stop having a stop codon at codon 580 results in loss of half of transmembrane domain (TMD) 11, TMD12, and a cytoplasmic tail, which might affect transport activity. In addition, novel variations, IVS12-1G>T at the splice acceptor site and -3A>C in the Kozak motif, were detected at 0.003 and 0.014 frequencies, respectively. Haplotype analysis using -11187G>A, -3A>C, IVS12-1G>T and 9 nonsynonymous variations revealed that the haplotype frequencies for **1b*, **5*, **15*, and **17* were 0.469, 0.000 (not detected), 0.037, and 0.133, respectively. These data would provide fundamental and useful information for pharmacogenetic studies on OATP1B1-transported drugs in Japanese.

Key words: ***SLCO1B1*; direct sequencing; novel genetic variation; amino acid change**

Received; July 18, 2007, Accepted; September 4, 2007

**To whom correspondence should be addressed*: Yoshiro SAITO, Ph.D., *Division of Biochemistry and Immunochemistry, National Institute of Health Sciences, 1-18-1 Kamiyoga, Setagaya-ku, Tokyo 158-8501, Japan. Tel. +81-3-5717-3831, Fax. +81-3-5717-3832, E-mail: yoshiro@nihs.go.jp*

†Present address: Department of Pharmacodynamics and Molecular Genetics, Faculty of Pharmaceutical Sciences, Iwate Medical University, 2-1-1 Nishitokuta, Yahaba-cho, Shiwa-gun, Iwate 028-3694, Japan.

‡Present address: Medical Oncology, Department of Medicine, Kobe University Hospital and Graduate School of Medicine, 7-5-2 Kusunoki-cho, Chuo-ku, Kobe 650-0017, Japan.

Introduction

Organic anion transporting polypeptide 1B1 (OATP1B1, also known as OATP-C, OATP2 and LST-1) is a liver-specific transporter expressed on the sinusoidal membrane and mediates uptake of various endogenous and exogenous compounds from blood into hepatocytes.[1,2] Exogenous compounds include several 3-hydroxy-3-methylglutaryl-coenzyme A reductase inhibitors (such as pravastatin), an active metabolite of irinotecan SN-38, methotrexate, and rifampicin; endogenous substrates include bilirubin and bilirubin glucuronide, cholate, leukotriene C_4, and estradiol-17β-glucuronide.[1,2]

OATP1B1 protein (691 amino acid residues) is encoded by *SLCO1B1*, which consists of 15 exons (including non-coding exon 1) and spans approximately 109 kb on chromosome 12p12.2-p12.1. Similar to other OATP family members, this transporter is predicted to have 12 transmembrane domains (TMDs).[1,3]

Several genetic polymorphisms and haplotypes with functional significance are already known in *SLCO1B1*. In Japanese, two haplotypes with nonsynonymous variations **1b* and **15* have been frequently reported. The *SLCO1B1*1b* haplotype with 388A>G (Asn130Asp) has been shown to have no altered transport activity from *in vitro* expression systems.[2,4-7] Recently, however, an *in vivo* study has suggested that the area under the concentration-time curve (AUC) of pravastatin is significantly lower in **1b/*1b* subjects than in **1a/*1a* subjects, suggesting increased transport activity possibly through increased protein expression.[8] Another major haplotype, *SLCO1B1*15* harboring both 388A>G (Asn130Asp) and 521T>C (Val174Ala), has been reported to show impaired plasma membrane expression[6] and reduced transport activity *in vitro*,[6,7] probably due to the Val174Ala substitution.[2,4,6] The association of the **15* haplotype with significant increases in AUC was reported for pravastatin,[2,9] and irinotecan and SN-38.[10] The haplotype frequencies of **1b*, **5* (with 521T>C, Val174Ala), and **15* were reported to be 0.46-0.54, 0.00-0.01, and 0.10-0.15, respectively, in Japanese.[5,11]

Recently, the *SLCO1B1*17* haplotype having 388A>G (Asn130Asp), 521T>C (Val174Ala), and -11187G>A was also shown to increase the AUC of pravastatin[9] and likely reduces the pravastatin efficacy on cholesterol synthesis,[12] although the effect of -11187G>A on transcriptional activity has not been clarified *in vitro*. The frequency of **17* has not, however, been reported in Japanese.

In this study, all 15 exons and their surrounding introns were resequenced for comprehensive screening of genetic variations in *SLCO1B1*. Sequence analysis detected 62 variations including 5 novel nonsynonymous ones from 177 Japanese subjects. Haplotype frequencies of **1b*, **5*, **15*, and **17* were also estimated.

Materials and Methods

Human genomic DNA samples: One hundred seventy-seven Japanese cancer patients administered irinotecan participated in this study and provided written informed consent. The ethical review boards of the National Cancer Center and the National Institute of Health Sciences approved this study. Whole blood was collected from the patients prior to the administration of irinotecan, and genomic DNA was extracted from blood leukocytes by standard methods.

PCR conditions for DNA sequencing and haplotype analysis: First, two sets of multiplex PCR were performed to amplify all 15 exons of *SLCO1B1* from 100 ng of genomic DNA using 1.25 units of *Z-Taq* (Takara Bio. Inc., Shiga, Japan) with 0.2 μM each of the mixed primers (Mix 1 and Mix 2) designed in the intronic regions as listed in **Table 1** (1st PCR). Mix 1 contained primers for amplifying exons 1 and 2, and 12 to 14, and Mix 2 contained primers for exons 3 to 7, 8 to 11, and 15. The first PCR conditions consisted of 30 cycles of 98 °C for 5 sec, 55°C for 10 sec, and 72°C for 190 sec. Next, each exon was amplified separately by *Ex-Taq* (0.625 units, Takara Bio. Inc.) with appropriate primers (0.5 μM) designed in the introns (**Table 1**, 2nd PCR). The conditions for the second round PCR were 94°C for 5 min, followed by 30 cycles of 94°C for 30 sec, 55°C for 1 min, and 72°C for 2 min, and then a final extension at 72°C for 7 min. For amplification of exons 10 and 13, PCR was carried out under the following conditions: 94°C for 5 min followed by 33 cycles of 94°C for 30 sec, 55°C for 1 min, and 72°C for 30 sec, and then a final extension at 72°C for 7 min. Following PCR, the products were treated with a PCR Product Pre-Sequencing Kit (USB Co., Cleveland, OH, USA) and directly sequenced on both strands using an ABI BigDye Terminator Cycle Sequencing Kit (Applied Biosystems, Foster City, CA, USA) with the sequencing primers listed in **Table 1** (Sequencing). Excess dye was removed by a DyeEx96 kit (Qiagen, Hilden, Germany), and the eluates were analyzed on an ABI Prism 3700 DNA Analyzer (Applied Biosystems). All variations were confirmed by sequence analysis of PCR products generated by new amplification of the original genomic DNA templates.

As of July 18, 2007, the novel variations reported here are not found in the database of Japanese Single Nucleotide Polymorphisms (http://snp.ims.u-tokyo.ac.jp/), dbSNP in the National Center for Biotechnology Information (http://www.ncbi.nlm.nih.gov/SNP/), or PharmGKB Database (http://www.pharmgkb.org/).

This study was supported in part by the Program for the Promotion of Fundamental Studies in Health Sciences of the National Institute of Biomedical Innovation, and the Health and Labor Sciences Research Grants from the Ministry of Health, Labor and Welfare.

Table 1. Primer sequences used in this study

		Amplified or sequenced region	Forward primer (5′ to 3′)	Reverse primer (5′ to 3′)	Amplified region[a]	Length (bp)
1st PCR	Mix 1	Exons 1 and 2	ACTCTGGGGCTAAAACCTATTGGAC	CTGCTTGCCATAACATCTTGAGGGT	14041049_14055679	14,631
		Exons 12 to 14	CTAGGGCTTTTATTGATAGGCAGGT	AAACTTCCAGACTGTCTTCTACCAT	14127745_14137752	10,008
	Mix 2	Exons 3 to 7	TTTGTTGAGAAGAGACTGTTAGGCA	GGAAAATGGATGAAGAAGCACTGGA	14083429_14092020	8,592
		Exons 8 to 11	AAGGACAGCACCAAGCAATGAAGGA	CATTCAACTCAGCAATCCCACTACC	14106917_14119592	12,676
		Exon 15	CTGAGGAGAACTGTAATTTGATGTC	TTTCCAGAGGCAAGCATTTACAACT	14148708_14152868	4,161
2nd PCR		Exon 1	TAACAGGCATAATCTTTGGTCT	AAGGGCTCAGAATGTAAGCG	14041915_14043281	1,367
		Exon 2	TCCTTAGGCTAGAATTTGTGT	CAAAGTGAGTCTCAAGACATT	14053227_14053950	724
		Exon 3	TGGCTGAGTAGTAGTACCTG	ATCCTCACTATCAACATTTTCA	14084394_14084961	568
		Exon 4	TGAGTGGTCTAATGTAGGTGA	AGGTGTAAGTGTTGAGGTCTT	14086324_14086946	623
		Exon 5	ATCTTTCTTGCTGGACACTTC	TATTAAGGAATTTGTTACAGGG	14088485_14089158	674
		Exons 6 and 7	CATAAGAATGGACTAATACACC	GGGAGACATTTTACATTTGGTT	14090310_14091202	893
		Exon 8	TTCCTAGACAGTATCTGTTGC	CTTCCACTTGTTATGTGCTCA	14108658_14109289	632
		Exon 9	AGTTACAAAACAGCACTTACG	TCAGGAACTCATCTAAAATAAG	14112156_14112798	643
		Exon 10	CAGGGGTTAAAACCTAGATGA	ATCCATGTATTTCTCTAAGCC	14114169_14114904	736
		Exon 11	TGGCAAAGATGGAGAGCGTA	AGTCAAATGAGGTGCTTCTTA	14117563_14118256	694
		Exon 12	TTGTCCAAAAGAGTATGTGCT	CAGCCTTGAGAGTTCATAGT	14128668_14129375	708
		Exon 13	TTGACCCAGCAATCCAACTAT	CCTTTTTTTTTTCATCATACCTAGT[b]	14133788_14134290	503
		Exon 14	ATATTAACCAACATAACTTCCA	CCTTGAATCACAGTTTCTTCG	14136297_14136980	684
		Exon 15	GATGGCTTAACAGGGCTTGA	TGCGGCAAATGATCTAGGAA	14150619_14151844	1,226
Sequencing		Exon 1	TAACAGGCATAATCTTTGGTCT	AAGGGCTCAGAATGTAAGCG		
			TATGTGAGAGAAGGGTCTGTA	CTACAGGTTACATTGGCATTT		
			AAATGCCAATGTAACCTGTAG	CTGAAATAAAGTACAGACCCT		
		Exon 2	TCCTTAGGCTAGAATTTGTGT	CAAAGTGAGTCTCAAGACATT		
		Exon 3	TGGCTGAGTAGTAGTACCTG	ATCCTCACTATCAACATTTTCA		
		Exon 4	TGAGTGGTCTAATGTAGGTGA	AGGTGTAAGTGTTGAGGTCTT		
		Exon 5	ATCTTTCTTGCTGGACACTTC	TATTAAGGAATTTGTTACAGGG		
		Exon 6	TTAAGAGTTTACAAGTAGTTAAA	AAGCAATTTTACTAGATGCCAA		
		Exon 7	CTTCTTTGTATTTAGGTAATGTA	ATAGTATAAATAGGAGCTGGAT		
		Exon 8	TTCCTAGACAGTATCTGTTGC	CTTCCACTTGTTATGTGCTCA		
		Exon 9	AGTTACAAAACAGCACTTACG	TCAGGAACTCATCTAAAATAAG		
		Exon 10	TTGATAGGTGCAGCAAACCAC	GGAATAAAAGAATGTGTTTGAG		
		Exon 11	TCTTTTTGATATATGTCTATCAT	AGTCAAATGAGGTGCTTCTTA		
		Exon 12	TTGTCCAAAAGAGTATGTGCT	CAGCCTTGAGAGTTCATAGT		
		Exon 13	GTTCTAACCACTTCCTCATAG	CCTTTTTTTTTTCATCATACCTAGT		
		Exon 14	TCCTTTTTACCATTCAGGCTTA	ACTAAAATGAGATACGAGATTG		
		Exon 15	GATGGCTTAACAGGGCTTGA	TGCGGCAAATGATCTAGGAA		
			CACATCTTTTATGGTGGAAGT	AGGCTTATTTATACTTCCACC		

[a]The reference sequence is NT_009714.16.
[b]Mismatched nucleotides at the 5′ end are underlined.

Furthermore, rare SNPs found in single patients as heterozygotes were confirmed by sequencing the PCR fragments produced by the amplification with a high fidelity DNA polymerase KOD-Plus- (TOYOBO, Tokyo, Japan).

Hardy-Weinberg equilibrium was analyzed by SNPAlyze version 3.1 (Dynacom Co., Yokohama, Japan). Estimation of *SLCO1B1* haplotypes was performed by an expectation-maximization based program, LDSUPPORT software.[13]

Results and Discussion

Sequence analysis from 177 Japanese subjects resulted in the identification of 62 genetic variations, including 28 novel ones (**Table 2**). Of these variations, 7 were located in the 5′-flanking region, 1 in the 5′-untranslated region (UTR), 13 in the coding exons (9 nonsynonymous and 4 synonymous variations), 5 in the 3′-UTR, and 36 in the introns. All detected variations were in Hardy-Weinberg equilibrium ($p > 0.05$).

Of the 9 nonsynonymous variations, 5 variations were novel: 311T>A (Met104Lys), 509T>C (Met170Thr), 601A>G (Lys201Glu), 1553C>T (Ser518Leu), and 1738C>T (Arg580Stop). All of these variations were found as heterozygotes with frequencies of 0.008 for 1738C>T (Arg580Stop) and 0.003 for the four other variations. Arg580, residing in TMD11, is conserved among human, rat and mouse OATP families.[1] The change from arginine residue to the immature termination codon leads to loss of this conserved amino acid

Table 2. Summary of *SLCO1B1* variations detected in this study

SNP ID			Reference	Location	Position		Nucleotide change	Amino acid change	Allele frequency (n=354)
This Study	dbSNP (NCBI)	JSNP			NT_009714.16	From the translational initiation site or from the end of the nearest exon			
MPJ6_SB1_001[a]				5′-flanking	14042128	-11355 (-1078)[b]	ccaatactctcaA/Gtaattaaccaag		0.003
MPJ6_SB1_002	rs4149015	ssj0003132	9, 15	5′-flanking	14042296	-11187 (-910)[b]	tatgtgtatacaG/Agtaaaagtgtgt		0.153
MPJ6_SB1_003[a]				5′-flanking	14042494	-10989 (-712)[b]	atctctactcaaG/Aaaaactttaac		0.076
MPJ6_SB1_004[a]				5′-flanking	14042530	-10953 (-676)[b]	cttcctttctccA/Tcaagtcaagtca		0.003
MPJ6_SB1_005	rs11835045			5′-flanking	14042793	-10690 (-413)[b]	atttgtcttaaaT/Ctatttcctattt		0.076
MPJ6_SB1_006[a]				5′-flanking	14042860	-10623 (-346)[b]	ttaaagaaaaaaA/-tcttatgccacc		0.003
MPJ6_SB1_007[a]				5′-flanking	14043018	-10465 (-188)[b]	aactaggttttaT/Catgtttgactag		0.003
MPJ6_SB1_008[a]				Intron 1	14043209	IVS1+65	ttcacggaagaaG/Cattttgatggtc		0.014
MPJ6_SB1_009	rs2010668	ssj0003141		Intron 1	14053267	IVS1-155	tcctacttttgtG/Ttccagcattgac		0.113
MPJ6_SB1_010[a]				5′-UTR	14053480	-3	atctatatttcaA/Ctcatggaccaaa		0.014
MPJ6_SB1_011[a]				Intron 2	14053635	IVS2+69	tagaaaagcaagT/Ctgttaaaaagaa		0.003
MPJ6_SB1_012[a]				Intron 2	14053648	IVS2+82	tgttaaaaagaaC/Tattatgtttcaa		0.003
MPJ6_SB1_013[a]				Intron 2	14053734	IVS2+168	aaaccagtctttT/Caatctgattaag		0.008
MPJ6_SB1_014	rs4149021	ssj0003142	9	Intron 2	14053759	IVS2+193	tatttctttggcG/Aaaatttttgatg		0.153
MPJ6_SB1_015	rs12812795		9	Intron 2	14053769	IVS2+203	gcgaaatttttgA/Ttgcttaatagtt		0.003
MPJ6_SB1_016[a]				Intron 2	14053807	IVS2+241	aatttagaaataT/Ctttgatagcttc		0.006
MPJ6_SB1_017	rs12303784			Intron 2	14053814	IVS2+248	aaatattttgatA/Ggcttctctttgg		0.003
MPJ6_SB1_018[a]				Intron 2	14084429	IVS2-129	aaagggaaaactA/Gagtatggttttt		0.003
MPJ6_SB1_019[a]				Intron 2	14084478	IVS2-80	aaagaagaaagcT/Cattataattcca		0.008
MPJ6_SB1_020	rs2291073	JST-043317		Intron 3	14084788	IVS3+89	actggggtaaatT/Gtatctctcacag		0.271
MPJ6_SB1_021	rs2291074	JST-043318		Intron 3	14084923	IVS3+224	attctataatgcA/Gcaaagaatgatg		0.243
MPJ6_SB1_022[a]				Exon 4	14086569	311	gttgtttcattaT/Agggaattggagg	Met104Lys	0.003
MPJ6_SB1_023	rs4149036	ssj0003160		Intron 4	14086714	IVS4+97	ataggcagttacC/Attttgagaagat		0.427
MPJ6_SB1_024[a]				Intron 4	14088523	IVS4-161	cacttttacccaT/Ccacatctcttaa		0.017
MPJ6_SB1_025	rs2306283	JST-063865	4, 5, 9, 11, 15	Exon 5	14088712	388	gaaactaatatcA/Gattcatcagaaa	Asn130Asp	0.667
MPJ6_SB1_026	rs2306282	JST-063864	11	Exon 5	14088776	452	ttttatcactcaA/Gtagagcatcacc	Asn151Ser	0.034
MPJ6_SB1_027	rs4149044	ssj0003170	9	Intron 5	14088970	IVS5+165	cacagttcgcccA/Tttaacaacacag		0.427
MPJ6_SB1_028	rs4149045	ssj0003171	9	Intron 5	14088994	IVS5+189	ggttaaactacG/Acgttttcacttc		0.429
MPJ6_SB1_029	rs4149046	ssj0003172	9	Intron 5	14088996	IVS5+191	tttaaactacgcG/Attttcacttcta		0.331
MPJ6_SB1_030	rs4149096	ssj0003230	9	Intron 5	14090372_14090377	IVS5-107_112	aaattacttgtaCTTGTA/-aattaaaaaaaa		0.427
MPJ6_SB1_031[a]				Intron 5	14090469	IVS5-15	aaatgaaacactC/Gtcttatctacat		0.003
MPJ6_SB1_032[a]				Exon 6	14090511	509	ctgggtcatacaT/Cgtggatatatgt	Met170Thr	0.003
MPJ6_SB1_033	rs4149056	ssj0003182	4, 5, 9, 11, 15	Exon 6	14090523	521	tgtggatatatgT/Cgttcatgggtaa	Val174Ala	0.175
MPJ6_SB1_034	rs4149057	ssj0003183	9, 11, 15	Exon 6	14090573	571	cccatagtaccaT/Ctggggctttctt	Leu191Leu	0.333
MPJ6_SB1_035[a]				Exon 6	14090578	576	agtaccattgggG/Actttcttacatt	Gly192Gly	0.003
MPJ6_SB1_036	rs2291075	JST-043319	9, 11, 15	Exon 6	14090599	597	cattgatgatttC/Tgctaaagaagga	Phe199Phe	0.427
MPJ6_SB1_037[a]				Exon 6	14090603	601	gatgatttcgctA/Gaagaaggacatt	Lys201Glu	0.003
MPJ6_SB1_038	rs2291076	JST-043320	9	Intron 7	14090961	IVS7+33	gtaccatgataaC/Tgtctttctaagc		0.336
MPJ6_SB1_039			11	Exon 9	14112452	1007	tccttactaatcC/Gcctgtatgttat	Pro336Arg	0.006
MPJ6_SB1_040[a]				Intron 9	14114331	IVS9-68	ttgacatacattG/Ctgtttcatctat		0.003
MPJ6_SB1_041	rs4149099	JST-080069	9	Intron 10	14117669_14117670	IVS10-106_-107	tttatctacttt-/CTTttttccctcttt		0.647
MPJ6_SB1_042			11	Intron 10	14117728_14117730	IVS10-46_-48	cttctttgtcttTTT/-cttctctctctc		0.003
MPJ6_SB1_043	rs4149070	ssj0003204	9	Intron 11	14128857	IVS11-170	gaaagaaatccaC/Gaaaactatttta		0.280
MPJ6_SB1_044	rs4149071	ssj0003205	9	Intron 11	14128938	IVS11-89	agtttgaacaagT/Cgagacttcacta		0.280
MPJ6_SB1_045	rs4149100	ssj0003234	9	Intron 11	14128952	IVS11-75	agacttcactaaA/-tataatgcaatg		0.395
MPJ6_SB1_046	rs4149072	ssj0003206	9	Intron 11	14128959	IVS11-68	actaaatataatG/Acaatgtatttgc		0.280
MPJ6_SB1_047			11	Intron 11	14129015	IVS11-12	catattttatacA/Gcaacgcttaagg		0.014
MPJ6_SB1_048[a]				Exon 12	14129082	1553	acagaaattactC/Tagcccatttggg	Ser518Leu	0.003
MPJ6_SB1_049	rs987839			Intron 12	14133812	IVS12-396	tccaactattggG/Atatctaccaaaa		0.316
MPJ6_SB1_050[a]				Intron 12	14134097	IVS12-111	ggggccattcaaC/Ttgtgagcttaat		0.020
MPJ6_SB1_051[a]				Intron 12	14134207	IVS12-1	tgtcttgtttcaG/Taattgttcaacc		0.003
MPJ6_SB1_052[a]				Exon 13	14134263	1738	tcaatggttataC/Tgagcactaggta	Arg580Stop	0.008
MPJ6_SB1_053	rs4149080	ssj0003214	9	Intron 13	14136533	IVS13-97	ctccaaatttttG/Caacttttattta		0.395
MPJ6_SB1_054	rs11045875		11	Intron 14	14136797	IVS14+50	gactatattaatT/Gcctaaaaaatat		0.011
MPJ6_SB1_055[a]				Intron 14	14150655	IVS14-232	tatatttttctcG/Attttatgaagaa		0.006
MPJ6_SB1_056[a]				Intron 14	14150656	IVS14-231	atatttttctcgT/Ctttatgaagaag		0.251
MPJ6_SB1_057[a]				Exon 15	14151004	1983	tgcatcagaaaaT/Cggaagtgtcatg	Asn661Asn	0.006
MPJ6_SB1_058[a]				3′-UTR	14151137	2116 (*40)[c]	tgtgtttccaaaC/Gagcattgcattg		0.011
MPJ6_SB1_059	rs4149085	ssj0003219		3′-UTR	14151264	2243 (*167)[c]	acaaactgtaggT/Cagaaaaaatgag		0.251
MPJ6_SB1_060	rs4149086	ssj0003220		3′-UTR	14151425	2404 (*328)[c]	aaacaaatgagtA/Gtcatacaggtag		0.025
MPJ6_SB1_061	rs4149087	ssj0003221	15	3′′-UTR	14151536	2515 (*439)[c]	gaactataatacG/Taaggcctgaagt		0.333
MPJ6_SB1_062	rs4149088	ssj0003222		3′-UTR	14151560	2539 (*463)[c]	tctagcttggatG/Atatgctacaata		0.333

[a]Novel variations detected in this study.
[b]Intron 1 is skipped for counting.
[c]Positions are shown as * and bases from the translational termination codon TAA.

along with the subsequent half of TMD11, TMD12 and the cytoplasmic tail,[1] which very likely affects transport activity. Other variations 311T>A (Met104Lys), 509T>C (Met170Thr), 601A>G (Lys201Glu), and 1553C>T (Ser518Leu) are located in TMD3, TMD4, the short cytoplasmic loop between TMD4 and TMD5, and the large extracellular loop between TMD9 and TMD10, respectively.[1] Using the PolyPhen program (http://genetics.bwh.harvard.edu/pph/) to predict the functional effects of the four amino acid substitutions, three substitutions, Met104Lys, Met170Thr and Ser518Leu, were expected to alter the protein function based on the PSIC (position-specific independent count) score differences derived from multiple alignments. The functional significance of these 5 novel nonsynonymous variations should be clarified in the future. In addition, a novel variation at the splice acceptor site, IVS12-1 G>T, was detected at a 0.003 frequency. This variation might cause aberrant splicing of *SLCO1B1* pre-mRNA and thus influence the expression level of active protein. Furthermore, -3A>C might reduce translational efficiency since this purine-to-pyrimidine alteration results in a deviation from the Kozak motif, where the purine nucleotide at position -3 from the translational initiation codon is important.[14]

Four known variations, 388A>G (Asn130Asp), 452A>G (Asn151Ser), 521T>C (Val174Ala), and 1007C>G (Pro336Arg), were detected at 0.667, 0.034, 0.175, and 0.006 frequencies, respectively, which are similar to the Japanese data reported previously.[5,11] The allele frequencies of 521T>C (Val174Ala) in Japanese (0.11–0.18) are comparable to those in other Asian populations (0.04–0.25) and Caucasians (0.14–0.22), but higher than that in African-Americans (0.02).[10,15,16] The frequencies of 388A>G (Asn130Asp) in Japanese (0.63–0.67) are also similar to those in other Asians (0.57–0.88) and African-Americans (0.75), but higher than those in Caucasians (0.30–0.51).[10,15,16] Variations 452A>G (Asn151Ser) and 1007C>G (Pro336Arg) have not been reported in other ethnic populations. Analysis of these four known variations with PolyPhen program showed that only Val174Ala was expected to alter protein function, which is consistent with the previous functional analysis.[2,4,6] Variations 1454G>T (Cys485Phe) and 1628T>G (Leu543Trp) previously reported in Japanese were not detected in this study.[11,17] Hepatocyte nuclear factor 1α is known to transactivate *SLCO1B1* through binding to the promoter region (from -10432 to -10420 from the translational start codon);[18] however, no variation was found in this region.

Using -11187G>A, -3A>C, IVS12-1G>T and 9 nonsynonymous variations, diplotype configuration was estimated for each subject. The configuration was estimated with >0.99 probabilities for all but four subjects. The predicted haplotype frequencies for **1b* [harboring 388A>G (Asn130Asp)], **5* [harboring 521T>C (Val174Ala)], **15* [harboring 388A>G (Asn130Asp) and 521T>C (Val174Ala)] and **17* [harboring -11187G>A, 388A>G (Asn130Asp), and 521T>C (Val174Ala)] were 0.469, 0.000 (not detected), 0.037 and 0.133, respectively. The haplotype frequencies for **1b* and **5* are similar to those in the previous studies in Japanese.[5,11] The **17* frequency is higher than those in Chinese (0.085), Finnish Caucasians (0.069), Malay (0.029) and Indians (0.009).[15,16] It should be noted that 76% (n=47 alleles) of 521T>C (Val174Ala)-bearing haplotypes were assigned as **17*, and 21% (n=13) of them as **15*. The remaining two (3%) was estimated to exist with 1007C>G (Pro336Arg) and **17* variations [-11187G>A, 388A>G (Asn130Asp), and 521T>C (Val174Ala)] on the same chromosomes. The **17* ratio in 521T>C (Val174Ala)-bearing haplotypes is similar to that in Chinese (65%), but higher than those in Finnish Caucasians (34%), Malay (26%) and Indians (14%).[15,16] Variation 452A>G (Asn151Ser, n=12 alleles) or 1738C>T (Arg580Stop, n=3) were predicted to be on the **1a* background (no other variation).

In conclusion, 62 genetic variations were identified, including 28 novel ones, in *SLCO1B1*. One novel nonsynonymous variation results in a truncated protein and four novel nonsynonymous variations result in amino acids substitutions. In addition, novel variations IVS12-1 G>T at the splice acceptor site and -3A>C in the Kozak motif were detected. Approximately 76% of 521T>C (Val174Ala)-bearing haplotypes were assigned as **17* and the majority of the remaining haplotypes were **15*. This information would be useful for pharmacogenetic studies to investigate the associations of *SLCO1B1* variations with interindividual differences in drug disposition.

Acknowledgments: The authors thank Ms. Chie Sudo for her secretarial assistance.

References

1) Hagenbuch, B. and Meier, P. J.: The superfamily of organic anion transporting polypeptides. *Biochim. Biophys. Acta.*, **1609**: 1–18 (2003).
2) Kivisto, K. T. and Niemi, M.: Influence of drug transporter polymorphisms on pravastatin pharmacokinetics in humans. *Pharm. Res.*, **24**: 239–247 (2007).
3) Tamai, I., Nezu, J., Uchino, H., Sai, Y., Oku, A., Shimane, M. and Tsuji, A.: Molecular identification and characterization of novel members of the human organic anion transporter (OATP) family. *Biochem. Biophys. Res. Commun.*, **273**: 251–260 (2000).
4) Tirona, R. G., Leake, B. F., Merino, G. and Kim, R. B.: Polymorphisms in OATP-C: Identification of multiple allelic variants associated with altered transport activity among European- and African-Americans. *J. Biol.*

Chem., **276**: 35669–35675 (2001).

5) Nozawa, T., Nakajima, M., Tamai, I., Noda, K., Nezu, J., Sai, Y., Tsuji, A. and Yokoi, T.: Genetic polymorphisms of human organic anion transporters OATP-C (SLC21A6) and OATP-B (SLC21A9): allele frequencies in the Japanese population and functional analysis. *J. Pharmacol. Exp. Ther.*, **302**: 804–813 (2002).
6) Kameyama, Y., Yamashita, K., Kobayashi, K., Hosokawa, M. and Chiba, K.: Functional characterization of SLCO1B1 (OATP-C) variants, SLCO1B1*5, SLCO1B1*15 and SLCO1B1*15+C1007G, by using transient expression systems of HeLa and HEK293 cells. *Pharmacogenet. Genomics*, **15**: 513–522 (2005).
7) Nozawa, T., Minami, H., Sugiura, S., Tsuji, A. and Tamai, I.: Role of organic anion transporter OATP1B1 (OATP-C) in hepatic uptake of irinotecan and its active metabolite, 7-ethyl-10-hydroxycamptothecin: *in vitro* evidence and effect of single nucleotide polymorphisms. *Drug Metab. Dispos.*, **33**: 434–439 (2005).
8) Maeda, K., Ieiri, I., Yasuda, K., Fujino, A., Fujiwara, H., Otsubo, K., Hirano, M., Watanabe, T., Kitamura, Y., Kusuhara, H. and Sugiyama, Y.: Effects of organic anion transporting polypeptide 1B1 haplotype on pharmacokinetics of pravastatin, valsartan, and temocapril. *Clin. Pharmacol. Ther.*, **79**: 427–439 (2006).
9) Niemi, M., Schaeffeler, E., Lang, T., Fromm, M. F., Neuvonen, M., Kyrklund, C., Backman, J. T., Kerb, R., Schwab, M., Neuvonen, P. J., Eichelbaum, M. and Kivisto, K. T.: High plasma pravastatin concentrations are associated with single nucleotide polymorphisms and haplotypes of organic anion transporting polypeptide-C (OATP-C, SLCO1B1). *Pharmacogenetics*, **14**: 429–440 (2004).
10) Xiang, X., Jada, S. R., Li, H. H., Fan, L., Tham, L. S., Wong, C. I., Lee, S. C., Lim, R., Zhou, Q. Y., Goh, B. C., Tan, E. H. and Chowbay, B.: Pharmacogenetics of SLCO1B1 gene and the impact of *1b and *15 haplotypes on irinotecan disposition in Asian cancer patients. *Pharmacogenet. Genomics*, **16**: 683–691 (2006).
11) Nishizato, Y., Ieiri, I., Suzuki, H., Kimura, M., Kawabata, K., Hirota, T., Takane, H., Irie, S., Kusuhara, H., Urasaki, Y., Urae, A., Higuchi, S., Otsubo, K. and Sugiyama, Y.: Polymorphisms of OATP-C (SLC21A6) and OAT3 (SLC22A8) genes: Consequences for pravastatin pharmacokinetics. *Clin. Pharmacol. Ther.*, **73**: 554–565 (2003).
12) Niemi, M., Neuvonen, P. J., Hofmann, U., Backman, J. T., Schwab, M., Lutjohann, D., von Bergmann, K., Eichelbaum, M. and Kivisto, K. T.: Acute effects of pravastatin on cholesterol synthesis are associated with SLCO1B1 (encoding OATP1B1) haplotype *17. *Pharmacogenet. Genomics*, **15**: 303–309 (2005).
13) Kitamura, Y., Moriguchi, M., Kaneko, H., Morisaki, H., Morisaki, T., Toyama, K. and Kamatani, N.: Determination of probability distribution of diplotype configuration (diplotype distribution) for each subject from genotypic data using the EM algorithm. *Ann. Hum. Genet.*, **66**: 183–193 (2002).
14) Kozak, M.: Possible role of flanking nucleotides in recognition of the AUG initiator codon by eukaryotic ribosomes. *Nucleic Acids Res.*, **9**: 5233–5252 (1981).
15) Pasanen, M. K., Backman, J. T., Neuvonen, P. J. and Niemi, M.: Frequencies of single nucleotide polymorphisms and haplotypes of organic anion transporting polypeptide 1B1 SLCO1B1 gene in a Finnish population. *Eur. J. Clin. Pharmacol.*, **62**: 409–415 (2006).
16) Jada, S. R., Xiaochen, S., Yan, L. Y., Xiaoqiang, X., Lal, S., Zhou, S. F., Ooi, L. L. and Chowbay, B.: Pharmacogenetics of SLCO1B1: Haplotypes, htSNPs and hepatic expression in three distinct Asian populations. *Eur. J. Clin. Pharmacol.*, **63**: 555–563 (2007).
17) Morimoto, K., Oishi, T., Ueda, S., Ueda, M., Hosokawa, M. and Chiba, K.: A novel variant allele of OATP-C (SLCO1B1) found in a Japanese patient with pravastatin-induced myopathy. *Drug Metab. Pharmacokinet.*, **19**: 453–455 (2004).
18) Jung, D., Hagenbuch, B., Gresh, L., Pontoglio, M., Meier, P. J. and Kullak-Ublick, G. A.: Characterization of the human OATP-C (SLC21A6) gene promoter and regulation of liver-specific OATP genes by hepatocyte nuclear factor 1α. *J. Biol. Chem.*, **276**: 37206–37214 (2001).

Nonplatinum-based Chemotherapy With Irinotecan Plus Docetaxel for Advanced or Metastatic Olfactory Neuroblastoma

A Retrospective Analysis of 12 Cases

Naomi Kiyota, MD[1]
Makoto Tahara, MD, PhD[1]
Satoshi Fujii, MD, PhD[2]
Mitsuhiko Kawashima, MD[3]
Takashi Ogino, MD[3]
Hironobu Minami, MD[4]
Ryuichi Hayashi, MD[5]
Atsushi Ohtsu, MD[1]

[1] Division of Gastrointestinal Oncology and Digestive Endoscopy, National Cancer Center Hospital East, Kashiwa, Chiba, Japan.

[2] Division of Pathology, National Cancer Center Hospital East, Kashiwa, Chiba, Japan.

[3] Division of Radiation Oncology, National Cancer Center Hospital East, Kashiwa, Chiba, Japan.

[4] Division of Oncology/Hematology, National Cancer Center Hospital East, Kashiwa, Chiba, Japan.

[5] Division of Head and Neck Surgery, National Cancer Center Hospital East, Kashiwa, Chiba, Japan.

Address for reprints: Naomi Kiyota, MD, Division of Gastrointestinal Oncology and Digestive Endoscopy, National Cancer Center Hospital East, 6-5-1 Kashiwanoha, Kashiwa, Chiba 277-8577, Japan; Fax: (011) 81-4-7131-4724; E-mail: nkiyota@east.ncc.go.jp

Received May 15, 2007; revision received August 25, 2007; accepted September 21, 2007.

BACKGROUND. The efficacy and safety of chemotherapy with irinotecan plus docetaxel were retrospectively evaluated for olfactory neuroblastoma.

METHODS. Twelve patients with histologically proven advanced or metastatic olfactory neuroblastoma were treated with chemotherapy with irinotecan plus docetaxel at the study institution between 2001 and 2005. Of these, 7 patients with locoregional disease and no prior radiotherapy received irinotecan plus docetaxel followed by definitive radiotherapy, 1 with photon radiotherapy and 6 with proton radiotherapy, whereas 3 patients with distant metastases and 2 with locoregional disease who had received prior radiotherapy received irinotecan plus docetaxel only.

RESULTS. The most common toxicities of ≥grade 3 among the 12 patients receiving irinotecan plus docetaxel were leukopenia (33%), neutropenia (50%), febrile neutropenia (8%), and diarrhea (25%), all of which were manageable. Partial response was achieved in 3 patients, giving an overall response rate of 25%. The response rate was higher in patients aged <50 years (3 of 4 patients) compared with those aged >50 years (0 of 8 patients) ($P = .018$). With a median follow-up period of 22.2 months, the median progression-free survival and overall survival were 13.6 months and 36.6 months, respectively. Of the 7 patients with locoregional disease also receiving definitive radiotherapy, the 2-year survival rate was 100% and 6 patients were alive at the time of last follow-up.

CONCLUSIONS. Chemotherapy for olfactory neuroblastoma with irinotecan plus docetaxel is safe and manageable. Patients aged <50 years may be sensitive to chemotherapy. Induction chemotherapy followed by definitive radiotherapy may represent a promising option for patients with locally advanced olfactory neuroblastoma. *Cancer* **2008;112:885–91.** © *2008 American Cancer Society.*

KEYWORDS: olfactory neuroblastoma, chemotherapy, irinotecan, docetaxel, proton radiotherapy.

Olfactory neuroblastoma (ONB), also known as esthesioneuroblastoma, is a rare tumor arising from the olfactory epithelium of the upper nasal cavity.[1,2] ONB accounts for 3% of all intranasal tumors[3] and its etiology is unknown. Since its first description by Berger and Luc in 1924,[4] approximately 1000 cases have been reported in the literature.[5] The sex distribution is roughly equal.[2,5] Although several authors have demonstrated a bimodal distribution in the age of diagnosis, with peaks in those aged 11 to 20 years and 51 to 60 years,[2,6] others have described a unimodal distribution concentrating in the fifth decade of life.[7]

DOI 10.1002/cncr.23246
Published online 11 January 2008 in Wiley InterScience (www.interscience.wiley.com).

With regard to treatment, the combination of surgery and radiotherapy is the most frequent approach and offers the highest cure rates,[8–12] but definitive radiotherapy as a nonsurgical treatment is also used.[2,10,12–14] However, despite definitive local treatment, local recurrence and distant metastases are often reported,[6,8,12] with the latter observed in 25% to 50% of cases.[15–19] Chemotherapy is therefore often also implemented in patients with recurrent or metastatic ONB. Experience at several institutions using various chemotherapeutic regimens has suggested that this tumor might be sensitive to chemotherapy,[7,8,18,20–22] but its rarity has prevented any clear determination of the role of chemotherapy or the optimal chemotherapy regimen.

Between 1995 and 2005, our group at the National Cancer Center Hospital East treated 20 patients with either or both advanced or metastatic ONB with chemotherapy. Results with a variety of chemotherapy regimens used before 2001, including platinum-based regimens,[23] were unsatisfactory, leading us to speculate on the possibility of using irinotecan plus docetaxel (ID). In addition, in patients with locoregional disease we adopted proton radiotherapy after induction chemotherapy with ID because of its lower radiotoxicity to adjacent tissues (brain, optic nerve, eyeball, etc).[24]

Investigation of this regimen in 3 ONB patients in a phase 1 study of ID for solid cancer produced a good response in 2.[25] The first, who had previously received platinum-based chemotherapy at our institution, was responsive to ID, with a response duration of approximately 10 months. The second, a chemotherapy-naive patient with locoregional disease, achieved a partial response with ID, and a subsequent complete response (CR) after proton radiotherapy after ID. We therefore decided to treat not only recurrent or metastatic ONB but also locoregional ONB with ID, and since 2001 have treated 12 patients with this regimen. Of these, 7 with locoregional disease and no prior radiotherapy received ID followed by definitive radiotherapy, namely, photon radiotherapy in 1 patient and proton radiotherapy in 6 patients.

In this retrospective analysis, we evaluated the efficacy and toxicity of chemotherapy with ID for ONB and the efficacy of ID followed by definitive radiotherapy for locally advanced ONB. After suggestions from several authors that the pathologic features of ONB might correlate with prognosis and response to chemotherapy,[1,10,18,26–28] we also analyzed the correlation between response and the histologic grading of Hyams.[28]

MATERIALS AND METHODS

We reviewed the clinical records of the 12 patients with ONB treated with ID at the National Cancer Center Hospital East between 2001 and 2005. All 12 had histologically proven ONB and pathologic specimens were available for 10 patients. These were reviewed according to the histologic grading system of Hyams[28], and the correlation between Hyams grade and response to ID was analyzed.

Response to chemotherapy was evaluated using the World Health Organization (WHO) standard response criteria.[29] Chemotherapy-related toxicities were graded by the National Cancer Center Institute Common Toxicity Criteria (version 2). Overall survival time was calculated from the initiation of chemotherapy with ID to the date of death or last follow-up, whichever occurred first. Progression-free survival time was calculated from the initiation of chemotherapy with ID to the documentation of progression or death. Actuarial survival was estimated by the Kaplan-Meier method.[30] Statistical analysis of categoric data was performed using a Fisher exact test. Differences were considered statistically significant at $P < .05$. All analyses were conducted using the statistical analysis software Stat View-J (version 5.0) for Windows (SAS Institute Inc, Cary, NC).

RESULTS

Patient Characteristics

Patient characteristics are summarized in Table 1. The 4 males and 8 females ranged in age from 24 to 73 years, with a median age of 58.5 years. According to the clinical staging system of Kadish and Wang,[1] 2 patients had stage B disease at the time of chemotherapy and 10 had stage C disease. The primary site was determined by either or both computed tomography scanning and magnetic resonance imaging. Intracranial invasion was noted in 5 patients, regional lymph node metastases in 6, and distant metastases in 3. The site of metastases in these 3 patients was the lung and liver; cervical lymph node, lung, and bone; and cervical lymph node and bone in 1 patient each. Of the 12 patients, 9 presented with locoregional disease and 3 initially presented with distant metastases. Of the 9 patients with locoregional disease, 2 had received prior radiotherapy, whereas 7 had not.

Of the 12 patients with histologically proven ONB, specimens for pathologic review were available for 10. Of these, 2 tumors were low grade (Hyams grade I/II) and 8 were high grade (Hyams rade III/IV).

TABLE 1
Patient Characteristics and Treatment Course in Individual Patients

Age, year	Gender	ECOG PS	Kadish stage	ICI	LR/DM	Metastatic site	Prior treatment	Chemotherapy	Response	Subsequent treatment	RT/PRT	Survival, months	Status
65	Woman	1	C	+	DM	L, H	S, RT	ID	PD	Chemotherapy	—	5.7	DWD
24	Woman	0	C	-	DM	LN, L, B	—	ID	PD	Palliative RT	—	6.5	DWD
36	Woman	1	C	+	DM	LN, B	S, chemotherapy, RT	ID	PR	Chemotherapy	—	22.5	DWD
54	Man	0	C	-	LR	LN	S, RT, chemotherapy	ID	NC	—	—	16.1	DWD
59	Woman	1	C	-	LR	LN	S, RT	ID	NC	—	—	29.7	AWD
73	Man	0	C	-	LR	—	S	ID	PD	PRT	CR	14.8	AWD
58	Woman	0	C	+	LR	—	—	ID	NC	PRT	CR	16.1	ANED
48	Woman	0	C	-	LR	LN	—	ID	PR	PRT	CR	19.6	ANED
61	Man	0	B	-	LR	—	—	ID	NC	RT	CR	22.2	ANED
66	Woman	0	B	-	LR	—	—	ID	NC	PRT	PR	36.6	DWD
32	Man	0	C	+	LR	—	—	ID	PR	PRT	CR	53.4	ANED
61	Woman	1	C	+	LR	LN	Chemotherapy	ID	NC	PRT, chemotherapy	PR	63.0	AWD

PS indicates performance status; ICI, intercranial invasion; LR, locoregional; DM: distant metastases; RT, radiotherapy; PRT, proton radiotherapy; ECOG, Eastern Cooperative Oncology Group; +, positive; L, lung; H, liver; S, surgery; ID, irinotecan plus docetaxel; PD, progressive disease; DWD, dead with disease; -, negative; LN, lymph node; B, bone; PR, partial response; NC, no change; AWD, alive with disease; CR, complete response; ANED, alive with no evidence of disease.

Treatment Results

Treatment results are also listed in Table 1. All 12 patients received chemotherapy with ID, given as 3 weekly administrations of both irinotecan at a dose of 50 to 60 mg/m^2 on Day 1 and docetaxel at a dose of 30 to 35 mg/m^2 on Day 1, repeated every 4 weeks. The recommended dose of this regimen had been previously determined as irinotecan at a dose of 50 mg/m^2 and docetaxel at a dose of 30 mg/m^2 in a phase 1 study at our institution.[25] Of the 12 patients, 3 had been recruited in this phase 1 study and the other 9 were treated with ID in clinical practice after the recommended dose had been determined. A median of 3 cycles of ID were given, ranging from 1 to 6 cycles. In the 7 patients with locoregional disease and no prior radiotherapy, the treatment plan called for ID followed by definitive radiotherapy. Radiotherapy was administered after a median of 3 cycles of ID (range, 1–6 cycles). One patient refused further administration of ID because his nasal bleeding was not improved after 1 cycle and he wished to receive definitive radiotherapy as soon as possible. A second patient received 6 cycles of ID because she wished to continue ID as long as a response was observed. The other 5 patients received 2 or 3 cycles of ID. Of the 7 patients, the 1 patients with Kadish stage B disease underwent definitive radiotherapy with photon radiation (total of 66 grays [Gy] in 2-Gy fractions), whereas the 6 patients with Kadish stage C disease received proton radiation (total of 65 cobalt Gray equivalents [GyE] in 2.5-GyE fractions).

All 12 patients demonstrated an assessable response to ID. Three of the 12 achieved a partial response (PR). One PR patient had distant metastatic disease and the other 2 PR patients had locoregional disease. The median progression-free survival was 13.6 months (range, 1.3–53.4 months) (Fig. 1). In the 7 patients with locoregional disease and no prior radiotherapy who received definitive radiotherapy after chemotherapy, 5 achieved a CR and 2 a PR.

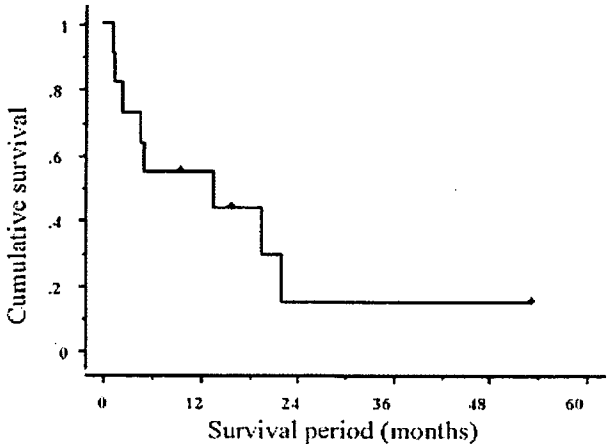

FIGURE 1. Progression-free survival (n = 12).

The median follow-up period in survivors was 22.2 months (range, 14.8–63 months). Estimated 1-year and 2-year survival rates were 83.3% and 53.3%, respectively. The median overall survival was 36.6 months (Fig. 2). The median survival of the 6 of 12 patients with recurrent or distant metastatic disease was 16.1 months (Fig. 3). Of the 7 of 12 patients with locoregional disease who had received no prior

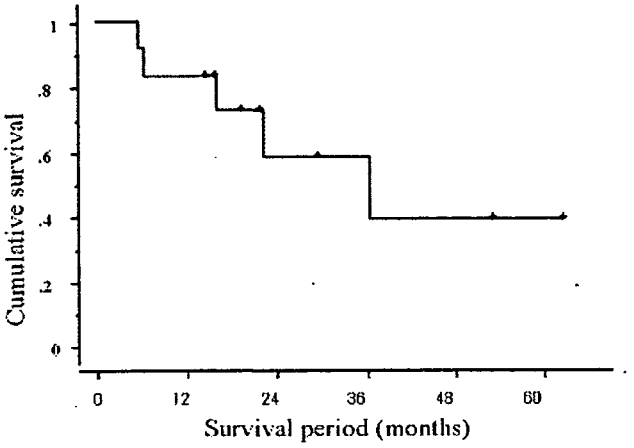

FIGURE 2. Overall survival (n = 12).

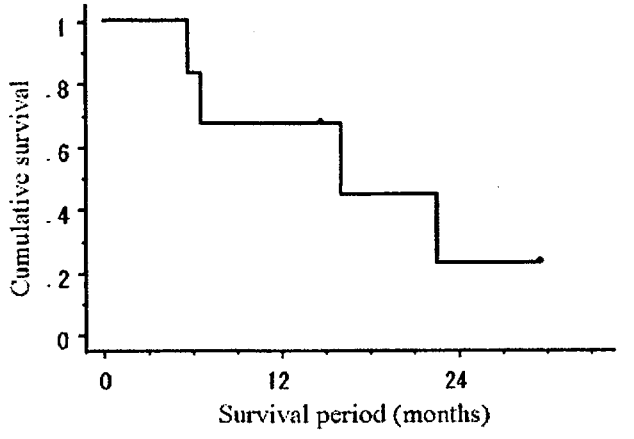

FIGURE 3. Survival in patients with recurrent or metastatic disease (n = 6).

radiotherapy, 1 received ID followed by photon radiation and 6 received ID followed by proton radiation. Among them, the 2-year survival rate was 100% and 6 patients were alive at the time of last follow-up (Fig. 4). Of the 5 CR patients who received definitive radiotherapy (1 with photon radiation and 4 with proton radiation), 4 patients were alive at the time of last follow-up with no evidence of disease. Toxicity of definitive photon or proton radiotherapy was mild and manageable. None of the 7 patients experienced treatment-related death or severe late toxicity due to irradiation, including vision impairment, brain necrosis, or others. Nevertheless, ongoing follow-up to ensure safety is required.

The most common grade 3 or 4 chemotherapy-related toxicities were leukopenia (33%), neutropenia (50%), febrile neutropenia (8%), and diarrhea (25%), all of which were manageable.

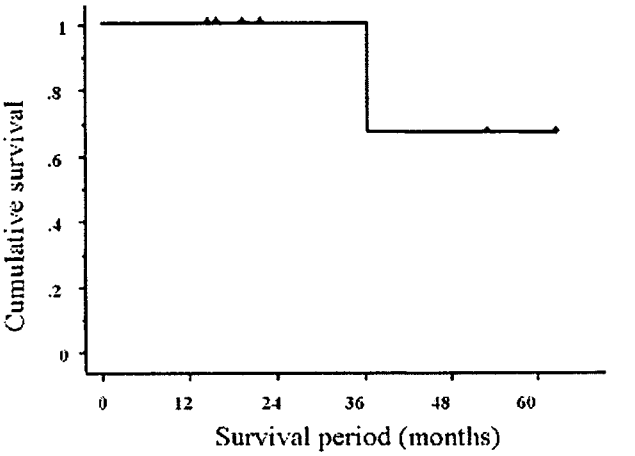

FIGURE 4. Survival in patients treated with irinotecan plus docetaxel followed by definitive radiation therapy (n = 7).

TABLE 2
Response According to Patient Characteristics

Characteristic	No.	No. of patients responding	*P*
Age <50 y	4	3	.018
Age ≥50 y	8	0	
Male	4	1	>.99
Female	8	2	
Distant metastasis			>.99
Present	3	1	
Absent	9	2	
Kadish stage B	2	0	>.99
Kadish stage C	10	3	
Intracranial invasion			.045
Present	5	3	
Absent	7	0	
Low Hyam grade (I/II)	2	0	>.99
High Hyam grade (III/IV)	8	3	

The correlation between response to chemotherapy and clinical and histologic variables is summarized in Table 2. The response rate to ID was 75% (3 of 4 patients) in the group aged <50 years, but was 0% (0 of 8 patients) in those aged >50 years ($P = .018$). Furthermore, the response rate was 60% (3 of 5 patients) in patients with intracranial invasion, but was 0% (0 of 7 patients) in those without ($P = .045$). Although the sample size was small, no response was observed (0 of 2 patients) in the Hyams low-grade (grade I/II) patients, whereas 3 responses were observed (3 of 8 patients) in the Hyams high-grade (grade III/IV) patients. No significant correlations between response to chemotherapy and other clinical variables were identified.